uOttawa

L'Université canadienne
Canada's university

FACULTÉ DES ÉTUDES SUPÉRIEURES ET POSTOCTORALES

uOttawa

L'Université canadienne
Canada's university

FACULTY OF GRADUATE AND POSDOCTORAL STUDIES

Sébastien Casault
AUTEUR DE LA THÈSE / AUTHOR OF THESIS

M.Sc. (Physics)
GRADE / DEGREE

Department of Physics
FACULTÉ, ÉCOLE, DÉPARTEMENT / FACULTY, SCHOOL, DEPARTMENT

Exact Enumeration Approach to Solving Transient Diffusion Problems Applied to Drug Delivery

TITRE DE LA THÈSE / TITLE OF THESIS

Dr. Slater
DIRECTEUR (DIRECTRICE) DE LA THÈSE / THESIS SUPERVISOR

CO-DIRECTEUR (CO-DIRECTRICE) DE LA THÈSE / THESIS CO-SUPERVISOR

EXAMINATEURS (EXAMINATRICES) DE LA THÈSE / THESIS EXAMINERS

Dr. Metzler

Dr. Hawrylak

Dr. Asner

Gary W. Slater
Le Doyen de la Faculté des études supérieures et postdoctorales / Dean of the Faculty of Graduate and Postdoctoral Studies

Exact Enumeration Approach to Solving Transient Diffusion Problems Applied to Drug Delivery

Sébastien Casault
B.Sc. University of Waterloo 2004

THESIS SUBMITTED IN PARTIAL FULFILLMENT
OF THE REQUIREMENTS FOR THE DEGREE OF
MASTERS OF SCIENCE IN PHYSICS

uOttawa

Your file Votre référence
ISBN: 978-0-494-49174-4
Our file Notre référence
ISBN: 978-0-494-49174-4

SUMMARY

This is a study of drug delivery problems from hydrogels and it is mainly focused on the effects of the hydrogel's geometry on the behaviour of the release profile. Studying drug delivery also offers one the opportunity to delve into the physical mechanisms involved in the release process to better understand its theoretical implications. We can apply the well-developed theory of diffusion in order to understand many aspects of drug delivery. Thus, this thesis starts with a presentation of concepts and theories used in the following two articles (chapters). We go over the basic concept of drug delivery, followed by an introduction on diffusion. We then explain the ideas governing drug release and how we have modeled it. The tools used to generate our drug release platforms are presented followed by a discussion on characterizing the resulting drug release profiles.

This thesis is presented as a series of two articles that have been submitted to peer-reviewed scientific journals. The first article presents a novel combinatorial technique used to obtain controlled drug delivery profiles. We use an exact enumeration diffusion model in order to obtain our drug release profiles and test its validity by comparing these results with analytical theory and widely used empirical tools. By using a genetic algorithm, we then show that it is possible to tailor the drug delivery platform in order to get a specific functional form of the release profile.

The second article consists in testing two widely used empirical functions that are used in the literature to characterize drug release profiles. Several claims have been made regarding the interpretation of these functions and we have used our exact enumeration data to argue that although the functions fit the data relatively well on certain time scales, they do not necessarily convey reliable information about the mechanism of release.

Finally, we conclude with preliminary work that was done on a second optimization technique to be used in controlling drug delivery profiles. The Metropolis simulated annealing was used to further optimize the design of the drug release platform and was shown to be quite effective, albeit being computationally demanding.

SOMMAIRE

Cette thèse vise à approfondir nos connaissances reliées au relâchement contrôlé de particules médicamenteuses confinées par des hydrogels polymériques. En particullier, nous utiliserons des simulations numériques pour systématiquement étudier l'impact de la géométrie et de la taille des fibres d'hydrogel sur les profils de relâchement des médicaments. De plus, nous examinerons les mécanismes physiques du processus d'échange de particules à l'interface hydrogel-solvant.

La thèse est divisée de la façon suivante. Le premier chapitre présente les concepts et théories pertinentes à la thèse; une présentation des concepts reliés au relâchement de particules dans les milieux poreux; une introduction à la théorie de la diffusion; une introduction au modèle numérique utilisé; et une revue des méthodes utilisées pour caractériser le relâchement des médicaments.

Les deux chapitres suivants consistent en deux articles soumis à des journaux scientifiques examinés par des pairs. Le premier présente un algorithme combinatoriel visant à contrôler le taux de relâchement de particules médicamenteuses. L'énumération exacte est utilisée afin d'obtenir les profils de relâchement qui sont ensuite comparés à des formules empiriques et des prédictions théoriques. En utilisant un algorithme génétique, nous démontrons également qu'il est possible de construire une structure d'hydrogel résultant en un profil de relâchement spécifique.

Le deuxième article présente une étude de deux fonctions empiriques couramment utilisées pour caractériser les profils de relâchements. En utilisant notre algorithme nous démontrons que, bien que les deux fonctions prédisent relativement bien les courbes de relâchement, leur paramètres n'apportent aucune information sur les mécanismes physiques du phénomène.

Pour conclure, nous présentons une étude d'une deuxième méthode d'optimisation du profil de relâchement. L'algorithme de refroidissement Metropolis est utilisé pour optimiser la concentration initiale de médicaments. Les résultats préliminaires démontrent que cette méthode est très efficace bien que l'algorithme requiert de grandes ressources informatiques.

STATEMENT OF ORIGINALITY

> Originality is the fine art of remembering what you hear but forgetting where you heard it.
> *(Laurence J. Peter, 1919–1988)*

The work presented in this thesis is, to the best of my knowledge and belief, new and original. Everything presented herein is my work except for the original creation of the enumeration model presented in Section 1.4.1. However, the application of the model and optimization algorithms towards diffusive drug delivery problems are part of my contribution – with the help of other members from our group.

The advances presented in this thesis are a result of my work during the last two years with the help of my supervisor and members of our research group. All analytical and numerical results presented here were obtained using my own Maple, MPI, and C++ codes. Some of the data analysis and graphical representation was performed using third party software (under consent) developed by Frédéric Tessier, a former member of our group.

ACKNOWLEDGEMENTS

Special acknowledgments go to my supervisor, Gary W. Slater for his enthusiastic support and expert advice. Thank you for the countless opportunities you have made available for me and the many re-reads; I owe you several red pens! I would like to thank members of the uOttawa Polymer Physics group; specifically Martin I, Martin II (you know who's who), and Eric for countless hours of useful discussions. Thanks mom and dad for having endured my numerous early and usually destructive "physics" experiments and for your continued encouragement. Thank you Cristina for your support and friendship.

Table of contents

1

Introduction

Facts are meaningless. You could use facts to prove anything that's even remotely true!
(Matt Groening/Homer Simpson, 1954–)

1.1 Bio-Chemical-Computational Physics

According to the magazine Fortune 500, the American pharmaceuticals industry constituted the fifth most profitable industry in percentage of revenues for the 2005 fiscal year in the US [1]. It is perhaps not surprising that in response to the market, many scientists who are usually associated with fundamental research gear their studies towards the development of novel pharmaceutic applications. Public institutions such as universities are also well suited to conduct studies in this field since they occupy a very unique position in society. University research can effectively be positioned at the forefront of cutting edge technology development while serving as a producer of knowledge outside the realm of industrial vested interests. This knowledge can then serve as an important tool when developing an efficient regulatory framework to be followed by the industrial sector [2]. Also, a multidisciplinary approach is crucial in order to conduct research in the field of pharmaceutics since there can often be huge gaps between fundamental research and practical application. For this reason, this thesis presents a study of fundamental physical concepts related to drug delivery problems while offering some experimental context making these principles readily applicable.

Drug delivery problems are particularly interesting since scientists must use principles usually associated with different fields such as biology and chemistry in order to understand how drugs are released into organisms and how they may react to environmental stimuli. Using this knowledge, a physicist concerned with drug delivery is often compelled to understand the fundamental interactions between the drug molecules and the environment (*e.g.*, the release platform, therapeutic surroundings, etc.). There are many analytical tools in a scientist's arsenal which help to elucidate underlying phenomena pertaining to drug delivery problems, specifically. For example, one can use the mathematical theory of diffusion in order to explain the behaviour of the molecules/particles involved in drug release. However, the associated equations are typically very complex (*i.e.*, unsolvable analytically) and require techniques borrowed from the field of computational science and statistics in order to be solved numerically, or exactly.

The goal of this thesis is to study certain aspects of diffusion related to drug delivery applications. Namely, we present a novel optimization scheme by which one can tailor the delivery platform in order to obtain a specific desired drug release profile. The diffusion process is modeled as a continuous time random walk (CTRW) of solute molecules on a lattice and is solved exactly using a numerical method explained in Section 1.4.1. The structure of our modeled drug delivery platform is optimized using a genetic algorithm created specifically for the purpose of this thesis. The computational engines required to perform most of the work presented in this thesis have been conceived and optimized to function in parallel on multiple processors using the Message Passing Interface (MPI) standard in C++ [3]. The results obtained from this research can be seen in Chapter 2. Using the exact enumeration method, we also present a study of drug release profile curves (*i.e.*, total drug release as a function of time). In Chapter 3, drug release profiles are compared and analyzed using empirical functions often used in the literature. We show that these fitting functions are sometimes improperly used as characterization standards and that they also do not convey underlying physical mechanisms, contrary to a widely held belief presented in the literature. Finally, in Chapter 4 we present a brief summary of preliminary research conducted by simultaneously using two optimization schemes in order to obtain tailored drug delivery platforms that exhibit improved controlled release.

Currently, there does not seem to be a clear theory or coherent foundation explaining drug delivery problems. This is not to say that the various components of this yet-to-exist unified theoretical framework are nonexistent. Drug delivery implicates many physical processes from a myriad of very active fields today – so much that it can seem overwhelming at first. For this reason,

the introductory section of this thesis will present key elements from these fields while offering an explanation pertaining to drug delivery specifically, in each case.

1.2 Drug delivery

Until relatively recently, therapeutic drug compounds have usually been delivered orally (in pill form or in suspension) or as injectables. However, we focus our studies on drug delivery through the use of polymeric hydrogels that can be placed on the skin (transdermal drug delivery) or swallowed and absorbed by the gastrointestinal (GI) tract. The use of hydrogels in drug delivery was promoted early in the 1980s [4, 5] and is now a common release platform used in controlled drug therapy [6–9]. Hydrogels consist of a three dimensional (3D) network of crosslinked polymers which swell and store relatively large quantities of water (in which drugs can be dissolved). The ability of a polymer network to hold water and swell is due to the presence of certain hydrophilic pendants along the backbone of the polymers [10]. The polar nature of these pendants assures that certain sections of the polymers repel each other thus creating relatively large pockets where water molecules are attracted and can be stored. Characteristics of the hydrogel such as water content (swelling), polymer and crosslinking densities can affect various properties such as rheology, surface kinetics, biocompatibility, etc. These characteristics are exploited to control the release of small particles (*e.g.*, therapeutic drug) from the hydrogel. For the purpose of this study, only hydrophilic drugs (*i.e.*, drug molecules that do not stick to or have affinity to any components of the drug release platform) will be considered here. The problem posed by hydrophobic drug molecules is however quite interesting and is currently a very active field of research in pharmacology (see reference [11] for an overview of the problem and several key results). Our hydrogel model and enumeration method is able to accommodate for effects associated with hydrophobic drug molecules and we propose some of the needed modifications to our model throughout the thesis.

Controlled drug release can be defined as the timely and opportune deployment of a certain therapeutic substance into a foreign environment [12]. This can be seen in Figure 1.1 where a therapeutic agent is being released in a patient's GI tract. The drug particles first undergo diffusion inside the hydrogel to reach its outer boundary where they are released in the organism. It is assumed that once the drug particles leave the hydrogel, they are instantaneously absorbed by the environment. In this thesis we concentrate on obtaining a constant rate of release over long periods

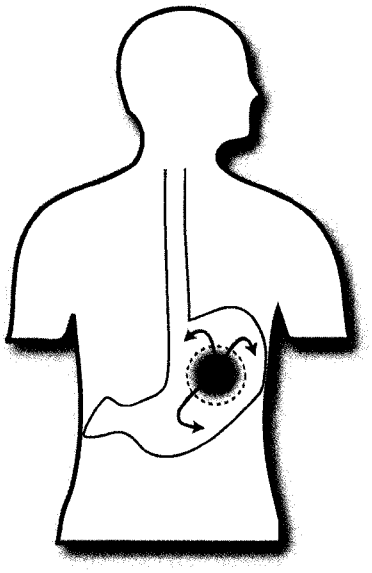

FIGURE 1.1 Schematic illustration of the concept of drug delivery from a swallowed hydrogel. Drug particles undergo diffusion (seen as a gradient) inside a circular hydrogel and are absorbed by the surrounding gastrointestinal tract (outward arrows), for example. Diffusion takes place inside the hydrogel and the outside environment acts as a perfect sink for the drug molecules.

of time, although obtaining release rates that are cyclic or triggered by environmental factors are also of great interest [13]. Controlling the rate of release, $\dot{M}(t)$, can help to maintain a drug in a therapeutic range while minimizing the risk of overdose. This allows for an improved systemic bioavailability of pharmaceutical substances leading to potentially fewer drug administrations by the patient, making optimal usage of a potentially costly substance. Figure 1.2 shows a typical release curve (solid line) from a simple drug release mechanism. This curve exhibits a strong peak followed by a slowly decaying tail which does not effectively keep the drug release rate within a favoured therapeutic range (dashed lines) throughout the duration of the dose. We would like to construct a hydrogel which could by design produce a release rate that is kept within a certain therapeutic range over the entire duration of a single dose (dotted line).

Drug release can occur via three main mechanisms if hydrophilic molecules in simple hydrogels are considered. Namely, by diffusion, by degradation of the hydrogel, or by swelling followed by diffusion. We will focus on diffusional release: the other two mechanisms will not be studied here. In normal diffusion for example, there is one free parameter which can depend (among other things) on the local structure of the environment, namely the diffusion coefficient. Diffusion can

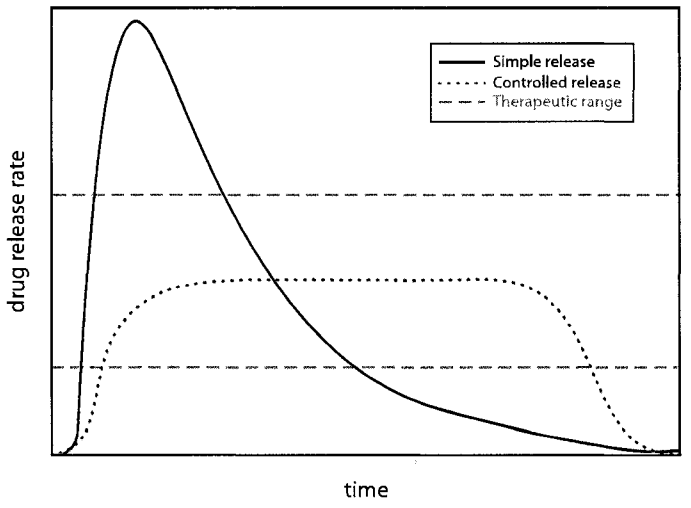

FIGURE 1.2 Schematic representations of two idealized release rates, $\dot{M}(t)$, as a function of time. A simple release may not be in the therapeutic range for the whole duration of the treatment (solid black). A controlled rate of release could increase the effective duration of the treatment, avoid potential overdosing, and reduce the number of required drug administrations. Figure inspired from [14].

thus be locally modulated since the drug particles take varying times to pass through different sections of the polymer matrix of the hydrogel (*i.e.*, avoiding the polymer chains which constitute the hydrogel). In our model, these chains will be represented by fixed obstacles which the particles will have to circumvent in order to diffuse to the outer surface of the hydrogel, at which point they are released into the outer environment (*i.e.*, perfect sink condition).

1.3 Diffusion

We begin by examining normal Fickian diffusion (sometimes referred to as Case I diffusion in pharmacology [1]). It is a transport mechanism by which matter or momentum spontaneously spreads in a material. It is a form of passive transport which requires no net energy and is a result of the

[1] There exist a classification scheme for diffusional drug release mechanisms from polymers which is used in the literature. In this scheme there are three general classes of diffusion behaviour: Case I diffusion is characterized by a drug release which occurs proportionally with the square-root of time (*e.g.*, Fickian diffusion). In Case II diffusion, the drug release is linearly proportional to time and in Super Case II diffusion, the drug release is proportional to some power of time greater than one [15].

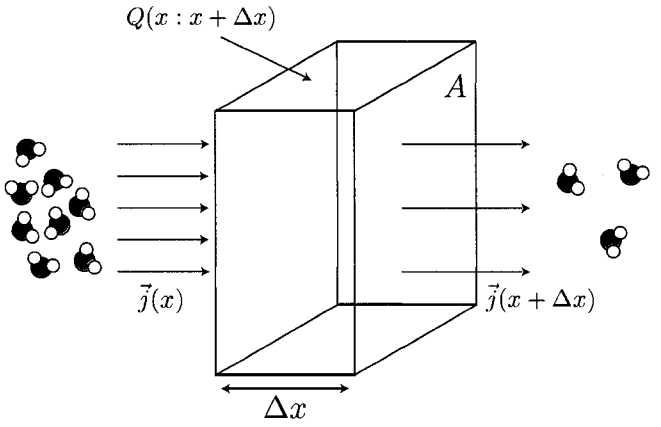

FIGURE 1.3 Schematic representation of the continuity equation in 3D. The quantity Q between points x and $x + \Delta x$ is conserved meaning that its rate of change between the same two points is solely due to the flux at points x and $x + \Delta x$.

second law of thermodynamics. This law states that the entropy of a closed system, S, which is not at equilibrium will increase (on average) over time,

$$\frac{\mathrm{d}S}{\mathrm{d}t} \geq 0. \tag{1.1}$$

Therefore, this law explains that particles in a region of high concentration will diffuse to a region of low concentration in order to increase the system's entropy. Reversing the process must always incur an expenditure of energy.

One can express diffusion mathematically with the use of a nonlinear partial differential equation. There are a few ways of obtaining this equation. One way of deriving this equation involves starting from the continuity equation (see Figure 1.3 for a simple 3D schematic illustration)

$$\frac{\partial \phi}{\partial t} = -\nabla \cdot \vec{j} \tag{1.2}$$

where $\vec{j}$ represents the flux of diffusing material and $\phi(\vec{r}, t)$ is the density function of the material at a spatial coordinate $\vec{r}$ and unit time t. Flux is a quantity, typically measured in $[n/At]$, which gives the number of molecules, n, that cross an area, A, per unit time, t. For illustrative purposes, let us assume that the density of a material only depends on x. We can write the quantity of material per unit volume found between points x and $x + \Delta x$ as $Q(x : x + \Delta x)$. We know that this quantity must be conserved while moving from point x to point $x + \Delta x$ (*i.e.*, no material is

created or destroyed) such that its rate of change between the two points is strictly due to the flux at the two points

$$\frac{\partial}{\partial t}Q(x : x + \Delta x) = \vec{j}(x)A - \vec{j}(x + \Delta x)A \,. \tag{1.3}$$

Dividing both sides by the the quantity Δx and rearranging gives

$$\frac{\partial}{\partial t}\frac{Q(x : x + \Delta x)}{\Delta x \cdot A} = -\frac{\vec{j}(x + \Delta x) - \vec{j}(x)}{\Delta x} \tag{1.4}$$

and taking the limit $\Delta x \rightarrow 0$ gives us Eq 1.2 (note that $Q(x : x + \Delta x)/A \cdot \Delta x = \phi(x)$ in this limit).

It is then possible to obtain an expression for $\vec{j}$ using Fick's first law [16] which makes the assumption that the flux of the diffusing material in a system is linearly proportional to the density gradient:

$$\vec{j}(\vec{r}, t) = -D\left(\vec{r}, \phi\right) \nabla\phi\left(\vec{r}, t\right), \tag{1.5}$$

$D\left(\vec{r}, \phi\right)$ is a function, which depends on position and density, known as the diffusion coefficient. By combining Eq 1.2 with Eq 1.5, the diffusion equation can be written in the form:

$$\frac{\partial\phi}{\partial t} = \nabla \cdot D\left(\vec{r}, \phi\right) \nabla\phi\left(\vec{r}, t\right) \,. \tag{1.6}$$

However, if the diffusion coefficient $D\left(\vec{r}, \phi\right)$ does not depend on the position nor the density, then the equation becomes linear and can be solved analytically under certain initial conditions:

$$\frac{\partial\phi}{\partial t} = D\nabla^2\phi\left(\vec{r}, t\right). \tag{1.7}$$

In the case of particles immersed in a fluid, diffusion is said to be the macroscopic representation of a microscopic process known as Brownian motion. The stochastic process of Brownian motion is a random walk of particles consisting of a series of uncorrelated steps. This random walk is due to the constant collision of the "walking" particles with fluid particles. These fluid particles obey the Maxwellian velocity distribution [17]:

$$P(v) = 4\pi\left(\frac{m}{2\pi k_B T}\right)^{3/2} v^2 \exp\left[\frac{-mv^2}{2k_B T}\right] \tag{1.8}$$

where $P(v)$ is the probability of having a particle of mass m with a velocity v (as usual, k_B is the Boltzmann constant and T is the temperature of the system). Diffusion is merely the continuum limit of a well-behaved (no bias or correlation) random walk [18]. Jan Ingenhousz was among the

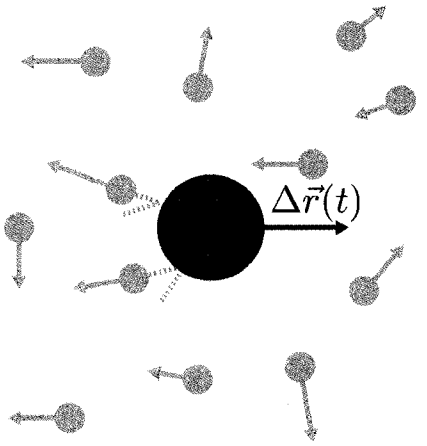

FIGURE 1.4 Schematic representation of a diffusing particle (dark grey) immersed in a fluid (light grey) in a closed system undergoing Brownian motion. The fluid particles have a Maxwellian velocity distribution indicated by arrows. There is no net motion of the fluid particles although the diffusing particle has a net motion, $\Delta\vec{r}(t)$, over a finite time scale.

first persons to observe this phenomenon in the 18^{th} century. However, the name comes from the Scottish botanist Robert Brown who, in 1827, studied the jittery motion of pollen particles in water and correctly identified that its mechanism was physical in origin and not biological as previously thought. A proper explanation of this phenomenon came in 1905 when Einstein established the relation between the diffusion coefficient of a Brownian particle and its friction coefficient [19].

It is possible to explain Brownian motion schematically (see Figure 1.4) as the net motion of a particle which is being bombarded by randomly moving fluid particles. Although the fluid particles have no time-averaged net motion, they can transfer momentum to the diffusing particle in a way such that it will have a net movement over a finite period of time. The diffusion equation (see Eq 1.7) is thus used to describe the bulk motion of these Brownian particles.

1.3.1 Sample solution in one dimension

Solving the diffusion in one dimension yields fundamental information about the nature of diffusional processes. One may take the one-dimensional diffusion equation,

$$\frac{\partial\phi(x,t)}{\partial t} = D\frac{\partial^2\phi(x,t)}{\partial x^2}\,, \tag{1.9}$$

where $\phi(x,t)$ is the probability of find a particle at point x at time t (note that $\phi(x,t)$ is used as a 1D function here). Performing a Fourier transformation with respect to x reduces the partial differential equation into an ordinary differential equation

$$\frac{\mathrm{d}\tilde{\phi}(k,t)}{\mathrm{d}t} = -Dk^2\tilde{\phi}(k,t)\,, \tag{1.10}$$

where $\tilde{\phi}(k,t)$ is the Fourier transform of $\phi(k,t)$ and k is a parameter which is essentially constant with respect to t. The solution is

$$\tilde{\phi}(k,t) = \tilde{\phi}(k,0)\exp\left(-Dk^2t\right)\,. \tag{1.11}$$

We now apply the initial condition $\phi(x,0) = \delta(x)$ which initially localizes all particles in a single location (*e.g.*, at the origin). The Dirac delta function translates as

$$\tilde{\phi}(k,0) = \int_{-\infty}^{\infty}\delta(x)\mathrm{e}^{ikx}\mathrm{d}x = 1\,, \tag{1.12}$$

in k space such that

$$\tilde{\phi}(k,t) = \exp\left(-Dk^2t\right)\,. \tag{1.13}$$

Applying the inverse Fourier transform then gives us the solution to the diffusion equation in one dimension

$$\phi(x,t) = \frac{1}{2\pi}\int_{-\infty}^{\infty}\exp\left(-Dk^2t\right)\mathrm{e}^{-ikx}\mathrm{d}k = \frac{1}{\sqrt{4\pi Dt}}\mathrm{e}^{-x^2/4Dt}\,. \tag{1.14}$$

For the point-source initial conditions chosen here (*i.e.*, $\phi(x,0) = \delta(x)$), normal diffusional processes thus evolve following a Gaussian distribution. The width of this Gaussian grows linearly with time, as indicated by the second moment (also called mean-square displacement or variance)

$$\langle x^2\rangle = \int_{-\infty}^{\infty}x^2\phi(x,t)\mathrm{d}x = 2Dt\,. \tag{1.15}$$

Note that $\langle x\rangle = 0$, since the integrand is an odd function of x.

1.3.2 Anomalous and other types of diffusion

Anomalous diffusion is best described by comparing it to normal diffusion. In normal diffusion, the mean-square displacement $\langle r^2\rangle$ of a particle increases linearly with time (as shown in the previous section)

$$\left\langle r^2\right\rangle = 2dDt\,, \tag{1.16}$$

where d is the dimensionality of the system. We can thus write the diffusion coefficient for long times as

$$D = \lim_{t \to \infty} \frac{\langle r^2 \rangle}{2dt} . \tag{1.17}$$

In disordered systems, we often have anomalous diffusion when the mean-square displacement of a particle does not increase linearly with time. Instead, we have

$$\langle r^2 \rangle \propto t^{2/d_w} \tag{1.18}$$

where d_w is the anomalous diffusion exponent ($d_w = 2$ corresponds to normal diffusion). It was de Gennes who first suggested the idea of analyzing transport phenomenon in disordered systems by performing random walks (diffusion) in percolation clusters [20]. Theoretical arguments have since been used to obtain Eq 1.18 which was later confirmed in various Monte Carlo simulations [21, 22]. In the presence of obstacles, $d_w > 2$ and diffusion is often slower (subdiffusion) than normal up to a certain period of time called the cross-over time, t_{CR}. For $d_w < 2$, diffusion is enhanced and is faster than for normal diffusion (superdiffusion). For example, Lévy flights are a type of motion which can be said to represent anomalous superdiffusion. In this case, the mean-square displacement grows faster than linearly with time due to an average step length chosen from a "heavy tail" distribution. The overall position of a particle is determined by the (infrequent) long steps, or *flights*, and there is no averaging out of the individual steps.

Our hydrogels have an associated obstacle concentration $0 < C_{\text{obst}} \leq C^*_{\text{obst}}$ without any biasing or kinetic effects. These obstacles will always slow the motion of the drug particles which means that we can only have cases of normal and subdiffusion when dealing with drug release from simple hydrogels. In most cases, the diffusion is anomalous at first and becomes normal for times above t_{CR} [24]. The cross over time increases with the associated obstacle concentration up to the percolation threshold (at the percolation threshold, $t_{CR} \to \infty$ for systems of infinite size). The percolation threshold, C^*_{obst}, is a critical value which gives the minimum concentration of obstacles (placed randomly) needed in an infinite system to form an obstacle barrier which spans the entire space (see Figure 1.5). This obstacle barrier essentially stops the diffusion process and $D = 0$ for $C_{\text{obst}} > C^*_{\text{obst}}$. The value of C^*_{obst} depends on the matrix geometry, the dimensionality of space, etc. This value can also be found for systems of finite size such as the ones studied here [25]. In these cases, it becomes important to perform averages over several "realizations of disorder" (*i.e.*, random obstacle configurations with similar concentration) and obtain proper statistical data.

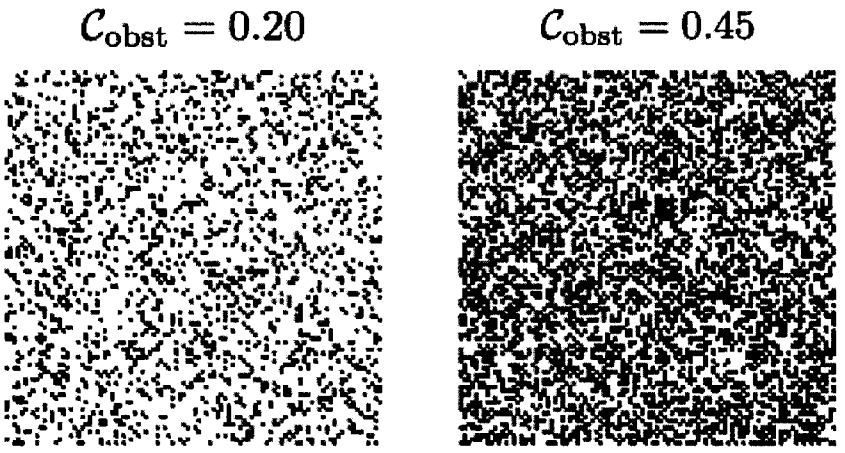

FIGURE 1.5 Two 100×100 square matrices. The percolation threshold for an infinite square matrix in 2D is $C^*_{obst} = 0.4069 \pm 0.0006$ [23]. Below the percolation threshold ($C_{obst} = 0.20$) we only have small isolated obstacle clusters. Above percolation ($C_{obst} = 0.45$) there is formation of obstacle barriers which span the entire space (an example is shown in red).

From the cross-over time one can obtain the associated cross-over length, R_{CR} (*i.e.*, the distance travelled by a particle before its diffusional behaviour passes from anomalous to normal):

$$R_{CR} = \sqrt{D_{t\to\infty}\left(C_{obst}\right) t_{CR}} \tag{1.19}$$

where $D_{t\to\infty}\left(C_{obst}\right)$ is the asymptotic value of the diffusion coefficient for a given obstacle concentration. Anomalous diffusion can been observed by plotting $\log\left[\langle r^2\rangle/t\right]$ versus $\log t$ (see Figure 1.6). These data are results from Monte Carlo simulations of diffusion for various values of C_{obst} on a 2D triangular lattice with a percolation threshold $C^*_{obst} = 0.5$. For the purpose of our argument, the same qualitative behaviour of the curves would be observed had the authors performed their calculations on a square lattice. The slanted fits of the curves represent anomalous diffusion with a slope of $2/d_w - 1$. Normal diffusion occurs in the sections shown with horizontal fits on this plot ($d_w = 2$). The intersection of the two lines formed from the two diffusion regimes for each simulation represents t_{CR}. For $C_{obst} = 0.00$, the diffusion is normal for all times whereas for $C_{obst} = C^*_{obst}$, the diffusion is anomalous for all times ($t_{CR} \to \infty$, $R_{CR} \to \infty$). For simulations with obstacle concentrations above C^*_{obst} the coefficient of diffusion is zero and only drugs located near the outer boundary of the hydrogel can actually exit due to the finite size of our systems.

These two different diffusional schemes (normal and anomalous) have a direct impact on the drug release behaviour as a function of time. For example, if the diffusional release of a drug

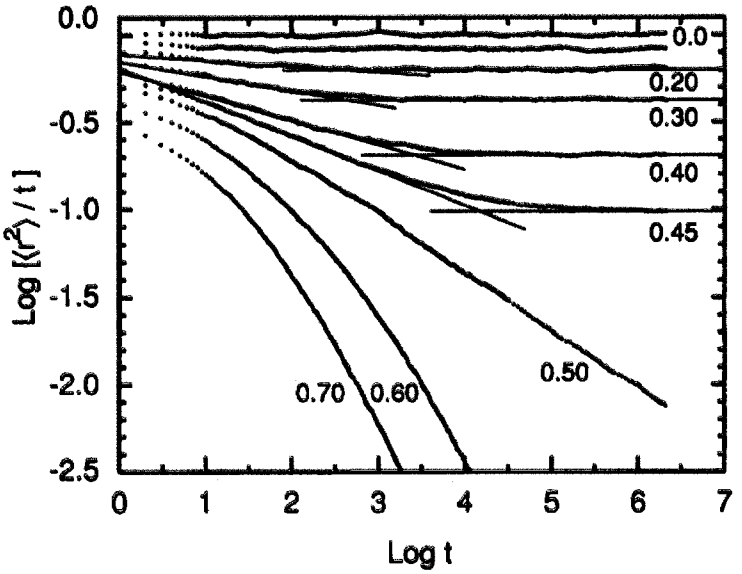

FIGURE 1.6 Manifestation of anomalous diffusion on a 2D triangular lattice ($C^*_{\text{obst}} = 0.50$). Diffusion is anomalous at first for moderate concentrations of obstacles (slanted fits) and becomes normal at increasing values of t (horizontal fits) up to $C_{\text{obst}} = 0.45$. For $C_{\text{obst}} = 0.00$, the diffusion is normal for the entire duration as represented by a horizontal line and for $C_{\text{obst}} = C^*_{\text{obst}}$, the diffusion is anomalous for all times. For $C_{\text{obst}} > C^*_{\text{obst}}$, the coefficient of diffusion is zero. Permission pending from the author and journal [24].

is constant with time, it is said to be of type Case II. Anomalous subdiffusion can apparently produce fractional release of a substance that is proportional with time [26] – in contrast with normal Fickian diffusion (Case I) where the release is proportional to the square-root of time. We will thus be interested in recreating situations where this behaviour may occur (*e.g.*, high obstacle concentrations, C_{obst}) since we wish to design drug delivery platforms which promote constant drug release.

1.3.3 Numerical modeling of diffusion

Brownian motion can be modeled numerically using a random walk model. The idea of the random walk is conceptually simple to understand and one can show that its statistical properties are identical to those of diffusion in the continuum limit [27]. The idea of performing a random walk to simulate diffusion was first popularized by the work of Montroll and Weiss in the 1960s [28]. The term random walk (sometimes called drunkard's walk) refers to the intuitive idea of performing a series of successive moves, each in random directions. The time between each successive move,

Δt, and the step length (equal to the lattice spacing here), a, remain constant for the duration of the entire walk in all our simulations.

Imagine a random walk in one dimension, where the probability of making a move to the right is p and the probability of making a move to the left is q and where $p = q = 1/2$. The probability of taking exactly n_{R} steps to the right, $P(n_{\mathrm{R}})$, after N steps is given by the binomial distribution

$$P(n_{\mathrm{R}}) = \frac{N!}{n_{\mathrm{R}}!(N - n_{\mathrm{R}})!} p^{n_{\mathrm{R}}} q^{N - n_{\mathrm{R}}} \tag{1.20}$$

which tends toward a Gaussian distribution for very large N

$$P(n_{\mathrm{R}}) \simeq \frac{1}{\sqrt{2\pi Npq}} \exp\left[-\frac{(n_{\mathrm{R}} - Np)^2}{2Npq} \right] . \tag{1.21}$$

The mean number of moves to the right and to the left are $\langle n_{\mathrm{R}} \rangle = Np$ and $\langle n_{\mathrm{L}} \rangle = Nq$, respectively. We can write the variance of this random walk as $\sigma_{\mathrm{R}}^2 = \langle n_{\mathrm{R}}^2 \rangle - \langle n_{\mathrm{R}} \rangle^2 = Npq$, or $\sigma^2 = Npqa^2$ if we use the step length. Eq 1.21 is similar to Eq 1.14 obtained in Section 1.3.1. Comparing the two allows us to write $\sigma^2 = 2Dt$ for a random walk:

$$\sigma^2 = Npqa^2 = \frac{a^2}{4} N = 2Dt . \tag{1.22}$$

Using $N\Delta t = t$, we have

$$\frac{a^2}{4} N = 2DN\Delta t \tag{1.23}$$

which finally gives us an expression for the diffusion coefficient that relates it to the step length and time interval between successive steps

$$D = \frac{a^2}{2\Delta t} . \tag{1.24}$$

We present in Section 1.4.1 a method of efficiently performing these random walks on finite-sized lattices.

1.4 Drug release

When studying diffusion related phenomena, many factors can influence the motion of particles. However, we are specifically interested in studying the release of hydrophilic drug particles from inside a hydrogel with absorbing (sink) boundary conditions. Since drug particles essentially "disappear" when they encounter the boundary, drug delivery is in fact a mean first passage time

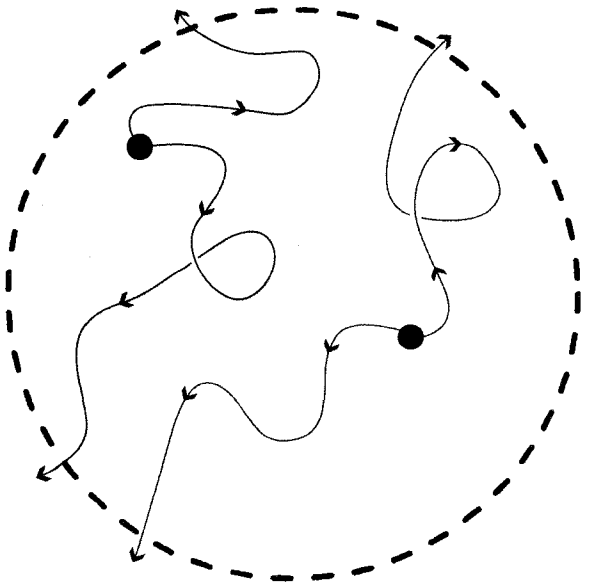

FIGURE 1.7 In discrete space, drug particles have a large but finite number of ways to escape a hydrogel through diffusion. Once such a particle reaches the outer boundary, it is absorbed. The particle will reach different locations on the boundary at different times depending on its trajectory and initial position. Since the boundary makes the particle vanish, we are only concerned by its first visit to the boundary. Shown here are two particles with two "first passages" to the outer boundary.

(MFPT) problem. A first passage time problem is characterized by a distinct change in behaviour of a parameter as it reaches a certain critical value for the first time. This is schematically illustrated in Figure 1.7 where two first passage trajectories of two drug particles to the outer boundary are shown. A release event occurs whenever a particle reaches the boundary, irrespective of the trajectory or initial condition. In discrete space (*i.e.*, on a lattice), the first passage probability, $F(\vec{r}, t)$, of finding a drug particle at a critical point (*i.e.*, the absorbing boundary, $\vec{r} = \vec{r_0}$) at time t fully describes the drug release process. This type of analysis allows one to study "extrema statistics" (*i.e.*, the time for some stochastic process to first reach a critical value) using powerful analytical tools [29].

The exact enumeration approach we use amounts to finding all the first passage times and associated probability distribution functions of the drug particles starting from any point within the hydrogel and going to the outer boundary. For reasons of simplicity in our model, collisions with fixed obstacles is the only mechanism by which we influence the diffusing particles. Drugs are assumed to be hydrophilic for simplicity (*i.e.*, do not stick to obstacles or to each other). This

is thought to be the main mechanism affecting the diffusion of our drug particles in real world experiments. We also restrain our studies to 2D systems since adding a third dimension would severely limit our capacity to perform simulations computationally due to the added size of the system. There are no particle-particle interactions and there is no external bias or internal viscosity gradient affecting the particles' motion or behaviour near obstacles. The obstacles represent polymer fibers in a given hydrogel, for example.

1.4.1 Exact enumeration methodology

As mentioned earlier, it is possible to obtain exact drug release profiles by using a technique based on the enumeration approach developed by Majid *et al.* [30] for solving random walk problems exactly. This adapted technique is explained in the following chapters and briefly expanded in this section.

Traditionally, the conventional Monte Carlo technique (MC) is employed to model diffusion on lattice-like structures [31, 32]. Data gathered from MC simulations generally tend to be rather noisy and converge somewhat slowly. There is also a lack of self-averaging which prevents one from obtaining better data by simply increasing the amount of Monte Carlo time steps (MCS) over which to perform statistical averages for random walk problems [33]. We can demonstrate the effectiveness of our approach with an example taken from a previous study [30] which follows the fractal dimension, d_w, as a function of algorithmic time step, N (see Figure 1.8) using the exact enumeration and compares it to data from MC calculations. This example performs random walks over a certain number of iterations and is averaged over typically 1000 percolation clusters in order to calculate d_w. The exact nature of the enumeration technique leads to a significant reduction in the error (solid line). The values of d_w are shown for both a square and triangular lattice. As shown, the data converges to the theoretically accepted value of $d_w = 4/3$ with no error bars using the enumeration scheme.

The enumeration method is best understood with an example (see Figure 1.9). The diffusion can be followed through four time steps in a 3×3, uniformly loaded hydrogel containing two obstacles ($C_{\text{obst}} = 2/9$). Uniformly loaded refers to the fact that all non-obstacle x, y sites are initially occupied by a uniform drug concentration, $C_{x,y}(0) = 1$. The cumulative release at each time step is also shown as the sum over all particle probabilities in the boundary, $M(t)$. This simple yet powerful technique can be described as follows: we compute all possible particle trajectories of a solute based on its initial location and its probability to diffuse to any first nearest neighbour

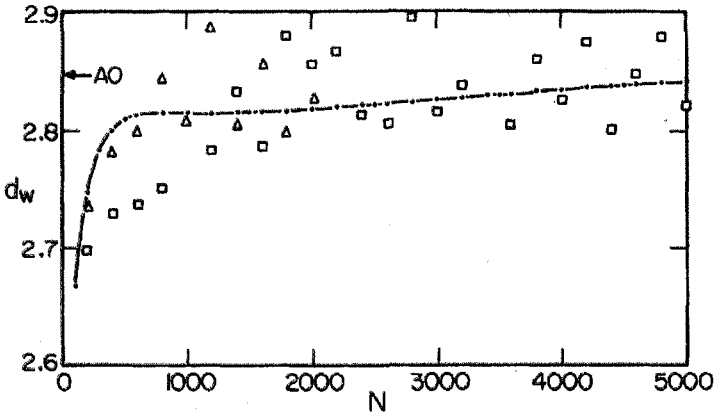

FIGURE 1.8 Fractal dimension, d_w, versus algorithmic iteration count, N, for a triangular lattice ($\triangle$), and for a square lattice ($\square$) obtained from Monte Carlo simulations together with the enumeration data ($-\bullet-$) of random walks on percolation clusters. One can see that the enumeration data is much cleaner while converging to the theoretical value for d_w. Reproduced with permission from [30] (pending).

(NN) from a lattice site j. Time is divided into small (finite) discrete intervals and all particles must attempt a jump at each time step. Such jumps are simply rejected (*i.e.*, the particle is reflected) if the neighbouring site is occupied by an obstacle (however, time is incremented even when jumps are rejected). For example, the drug probability density function P_j at time $t+1$ (assuming no neighbour is an obstacle) can be written as:

$$P_j(t+1) = \sum_{i=1}^{z(j)} P_i(t) p_{i,j} \tag{1.25}$$

where i is summed over all NN of lattice site j, $z(j)$ is the coordination number for the lattice, and $p_{i,j}$ is the probability to diffuse from site i to j. In an isotropic and unbiased system, a given solute particle has an equal probability of diffusing to any four of the NN: $p_{\pm x} = p_{\pm y} = 1/4$.

We can write Eq 1.25 specifically for the case of drug diffusion with obstacles (the value of $p_{i,j}$ is 0 if there is an obstacle on site j) in Cartesian coordinates with drug density function $C_{x,y}$ as

$$\begin{aligned} C_{x,y}(t+1) &= \left[C_{x-1,y}(t)(1-q_{x-1,y}) + C_{x,y}(t)q_{x+1,y}\right] p_{+x} \\ &+ \left[C_{x+1,y}(t)(1-q_{x+1,y}) + C_{x,y}(t)q_{x-1,y}\right] p_{-x} \\ &+ \left[C_{x,y-1}(t)(1-q_{x,y-1}) + C_{x,y}(t)q_{x,y+1}\right] p_{+y} \\ &+ \left[C_{x,y+1}(t)(1-q_{x,y+1}) + C_{x,y}(t)q_{x,y-1}\right] p_{-y}. \end{aligned} \tag{1.26}$$

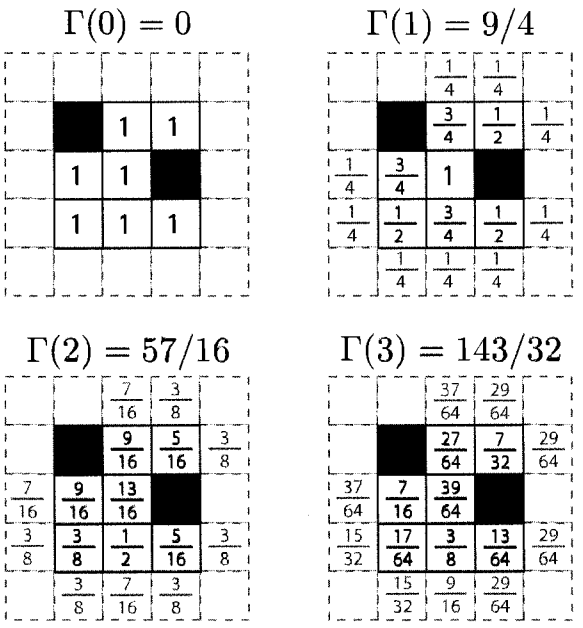

FIGURE 1.9 Diffusion from a uniformly loaded hydrogel with uniform initial drug concentration $C_{x,y}(0) = 1$ and two obstacles. The concentration of obstacles is $C_{\text{obst}} = 2/9$. The cumulative amount of drug released after each time step is shown in grey for each boundary site, and the sum $M(t)$ is given in all cases.

Here, $q_{x,y}$ is a site occupation index whose value is 1 if the site (x, y) is occupied by an obstacle and 0 if not. Since we are dealing with non-degradable hydrogels, the value of $q_{x,y}$ is fixed for all t and is determined by the initial structure of the hydrogel. Also, as schematically illustrated in **Figure 1.9**, the calculation is done iteratively, starting with a given initial drug concentration distribution $C_{x,y}(0)$; in this example $C_{x,y}(0) = 1 \ \forall \ x, y$ if the site is not occupied by an obstacle.

Release from the finite-sized hydrogel is thus modeled by imposing absorbing boundary conditions $p_{\pm x} = p_{\pm y} = 0$ on the outer surface of the structure. Once a drug concentration has reached the outer surface, it cannot diffuse back inside and the cumulative amount is the sum of all those probabilities which have crossed this boundary up to time t (see Figure 1.9).

Using discretized notation, we can write the mean-square displacement of a particle as

$$\left\langle r^2 \right\rangle (t) = \sum_j P_j r_j^2 (t) \tag{1.27}$$

where r_j is the magnitude of the particle's position at time t. This quantity could be useful for studying parameters such as the cross over length and time or the diffusion process using an infinite lattice. We can group the local drug concentrations, $C_{x,y}(t)$, into a column vector with s elements (one for each lattice site), $|C(t)\rangle$. We can then write Eq 1.26 as a matrix equation

$$|C(t+1)\rangle = \mathbf{T}|C(t)\rangle \tag{1.28}$$

where $\mathbf{T}$ is an $s \times s$ Markovian matrix which transforms the drug distribution of time t into the one at time $t+1$ ($\mathbf{T}$ includes all the information about the location and behaviour of the diffusing particles at the obstacles and at the boundary). In stochastic probability theory Markovian refers to a process by which the probability distribution of future states, given the present and all past states, depends only upon the current state and not on any past states [34].

This enumeration approach has been used many times to model diffusion related problems in various media. It has been used to study diffusion on percolation backbones [35], on diffusion limited aggregates (DLA) [36], trapping particles in 1D [37], in 2D and 3D [38], etc.

1.4.2 Diffusion coefficients

As mentioned before in Section 1.2, the diffusion coefficient is used to describe the behaviour of particles undergoing normal diffusion. We will show in the next section that it is possible to obtain a solution to the diffusion equation for a 2D circular disk as long as one knows the diffusion coefficient for the particles inside the gel. Let us then mention a scheme one may use to obtain these diffusion coefficients for use in the analytical theory. Using results previously obtained by members of our group, we can obtain exact values of the steady-state scaled diffusion coefficient, D^*, for particles undergoing diffusion in hydrogels of various obstacle concentrations, $\mathcal{C}_{\text{obst}}$, below the percolation threshold [39–41]. For analytic purposes, we replace a given concentration of obstacles by a uniform effective viscosity (*i.e.*, an effective (or scaled) diffusion coefficient D^* which models the retarded diffusive motion of the particles). The effective diffusion coefficient is:

$$D^* = \frac{D}{D_0} \tag{1.29}$$

where D_0 is the diffusion coefficient in the absence of obstacles (or between the obstacles). The percolation threshold for a 2D infinite square lattice of coordination number $z = 4$, is $\mathcal{C}^*_{\text{obst}} =$

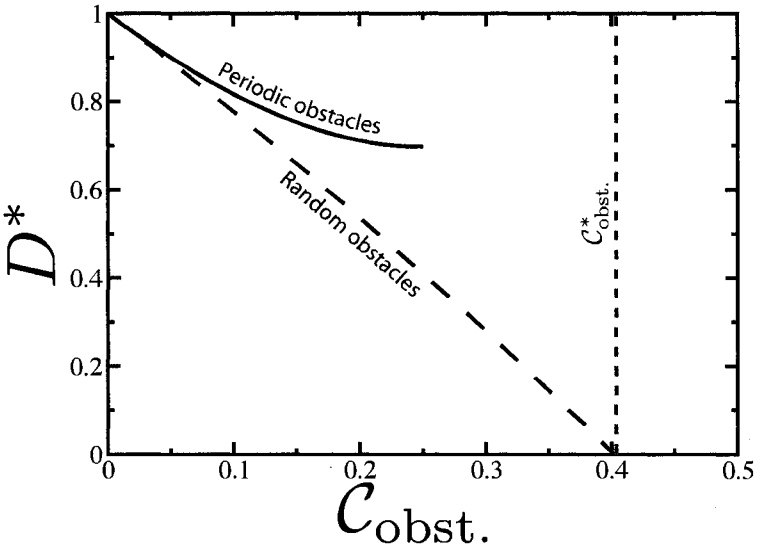

FIGURE 1.10 Scaled diffusion coefficient $D^* = D/D_0$, as a function of obstacle concentration, C_{obst}. The solid line is for a hydrogel with periodically placed obstacles and the dashed line is for a hydrogel with randomly placed obstacles. The periodic systems stop at $C_{obst} = 1/4$ since this is the highest concentration attainable on a square lattice. As expected, for random systems, D^* goes to 0 as C^*_{obst} is reached.

0.4069 ± 0.0006 [23]. For such a 2D hydrogels with obstacles placed periodically, it was shown that:

$$D^* \simeq \frac{1 - \pi C_{obst} + \frac{\pi^2}{2} C^2_{obst} + \dots}{1 - C_{obst}} \tag{1.30}$$

and for hydrogels with randomly-placed obstacles:

$$D^* \simeq 1 - (\pi - 1)\, C_{obst} - 0.8558 C^2_{obst} + \dots . \tag{1.31}$$

The values of D^* for systems composed of randomly placed obstacles are lower than in systems composed of periodically placed obtacles (see Figure 1.10) for given obstacle concentrations. This is presumably due to the formation of various structures in the random system which further hinder the motion of particles (*e.g.*, traps, walls, long tortuous channels). These equations assume pure Fickian diffusion. These exact values will also allow us to compare our numerical results to theory at low obstacles concentrations and help gauge the accuracy of our diffusion model.

1.4.3 Analytical solution

It is possible to obtain an analytic solution to the equation of diffusion for certain uniformly loaded round hydrogel geometries [42]. This has a significant importance since it allows comparison of the drug release profile obtained from our enumeration to the exact analytical theory. The enumeration results are shown to be in perfect agreement with the theory in the following chapters for hydrogels in the low obstacle concentration limit. The theory assumes a homogeneous coefficient of diffusion throughout the hydrogel which allows us to solve the diffusion equation analytically. However the coefficient of diffusion is highly dependent on $\vec{r}$ in hydrogels with higher obstacle concentrations and there is no longer an analytical solution to this nonlinear version of the equation. More importantly, the functional form of $D^*(\vec{r})$ itself is not known and depends on the placement of the obstacles which further prevents us from solving the equation numerically as well (except, potentially, for specific realizations of disorder).

As an example, we can obtain an analytic expression for drug release through diffusion from a 2D uniformly loaded circular hydrogel with an initial uniform concentration of drug on every non-obstacle site. The 2D, angular symmetric equation of diffusion written in polar coordinates is:

$$\frac{\partial C(r,t)}{\partial t} = D^* \left(\frac{\partial^2}{\partial r^2} + \frac{1}{r}\frac{\partial}{\partial r} \right) C(\vec{r},t) \tag{1.32}$$

where $C(\vec{r},t)$ describes the drug concentration at position $\vec{r}$ at time t (D^* is defined in Eq 1.29). We impose the following boundary conditions

$$C(r,0) = \mathcal{H}(r-r_0)C_0 \tag{1.33}$$

$$C(r_0,t) = 0, \tag{1.34}$$

where $\mathcal{H}$ is the Heaviside function, and C_0 is the initial drug concentration of the free sites inside the capsule. Equation Eq 1.34 accounts for the absorbing boundary located at r_0 (the radius of the circular hydrogel).

The solution to equations Eq 1.32 – Eq 1.34 is

$$C(r',t) = \sum_{n=1}^{\infty} C_n(r_0) J_0(\lambda_n r') \exp\left[-D^* \left(\frac{\lambda_n}{r_0} \right)^2 t \right] \tag{1.35}$$

where J_0 is the 0^{th} order Bessel function of the first kind, λ_n represents the n^{th} zero of $J_0(r)$ (refer to Chapter 2 for sample values), $r' = r/r_0$ is a scaled radial position, and the coefficients,

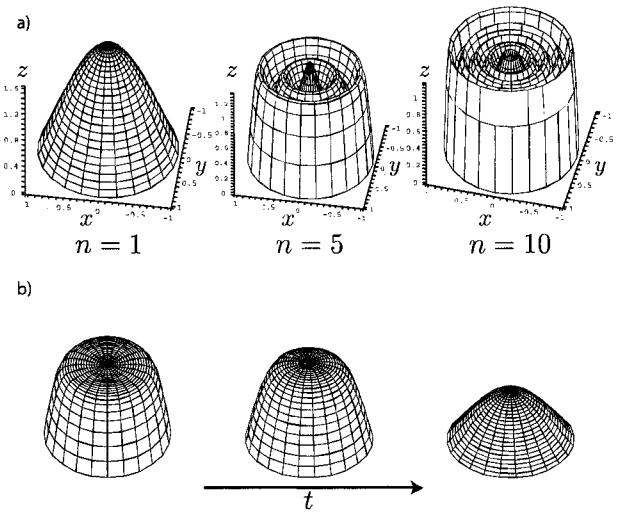

FIGURE 1.11 This shows in a) the initial state of a circular hydrogel (xy plane). The initial drug concentration, $C(\vec{r}, 0)$, is shown on the z-axis as a function of the number of terms, n, used in the series solution presented in Eq 1.35. The drug concentration as a function of time can be seen in b) for $n = 5$.

$C_n(r_0)$, are given by:

$$C_n(r_0) = \frac{2C_0}{J_1^2(\lambda_n)} \int_0^1 \mathcal{H}(r - r_0) J_0(\lambda_n r') r' \, \mathrm{d}r'. \tag{1.36}$$

We notice the effect of adding more terms on the initial drug concentration distribution (see Figure 1.11a). In this figure, the circular hydrogel is shown on the xy plane as well as the initial drug concentration (on the z-axis). Adding more terms to the series increases the level of definition such that the hydrogel is more accurately modeled. Bessel functions are notoriously poor at representing sharp features. For this reason, ≥ 5 terms are usually kept in the series expansion when using data from the analytic solution. We can see the time progression of the drug distribution in Figure 1.11b for the case of $n = 5$. The solution to Eq 1.35 is then integrated over the area (or volume in three dimensions) of the hydrogel, Ω, and over time in order to obtain the drug release curve.

$$M(t) = M_0 - \int_0^t \int_\Omega C(\vec{r}, t') \mathrm{d}\Omega \mathrm{d}t' \tag{1.37}$$

where $M_0 \equiv \int_\Omega C(\vec{r}, 0) \mathrm{d}\Omega$ represents the total initial amount of drugs present in the hydrogel (note that $M(0) \neq M_0$ using this notation). This solution allows us to obtain an exact release profile from a circular disk with a homogeneous coefficient of diffusion in order to test the validity

of our exact enumeration. The enumeration provides release curves which are in remarkable agreement with this theory as one can conclude from the results presented in Chapter 2. However, as mentioned earlier, the analytical solution begins to break down as C_{obst} approaches the percolation threshold. In other words, the assumption that we can replace the obstacles by an effective viscosity (or diffusion coefficient D^*) is valid for $R_{CR} \ll r_0$ and, since our hydrogels have a finite (read small) sizes, only applies at low obstacle concentrations. Figure Figure 1.6 can be interpreted to show R_{CR} as a function of C_{obst} to predict the minimum size of a hydrogel needed to use the exact value of D^* obtained in Section 1.4.2. As one increases C_{obst}, the system size must also increase in order to avoid complications due to anomalous diffusion. The onset of anomalous diffusion and increasing positional dependence of D^* is the main reason for having to use the enumeration method in order to study hydrogels for use in drug delivery as opposed to simply solving the diffusion equation for various values of D^* – which could not change the functional form of the drug release profile.

1.5 Genetic optimization

Genetic algorithms, as the name suggests, are a class of combinatorial optimization methods which use traits inspired from evolutionary biology in order to converge to an optimum. The study of cellular automata inspired John Holland at the University of Michigan to theorize about these algorithms in the late 1960's [43, 44]. Since then, these heuristic algorithms have been successfully applied to a myriad of complex problems such as the classic traveling salesman problem [45], scheduling optimizers [46], protein folding, etc. In Chapter 2, we use a genetic algorithm in order to create a hydrogel structure which exhibits constant release rate characteristics. Here we are trying to find the optimal obstacle placement which give our desired release rate. A genetic algorithm allows us to intelligently "try" a large number of obstacle configurations and systematically converge to a satisfactory solution.

A typical genetic algorithm usually comprises four main steps: the initialization of a population, the selection of fit candidates, the reproduction of these candidates, and the termination when a specific condition has been met. In the initialization phase, a population composed of individuals is created. Each individual is created with a specific number of chromosomes (*e.g.*, a specified section of each hydrogel with a unique obstacle concentration). Once a population is formed, the individuals are ranked according to a fitness parameter. This fitness parameter is usually a simple

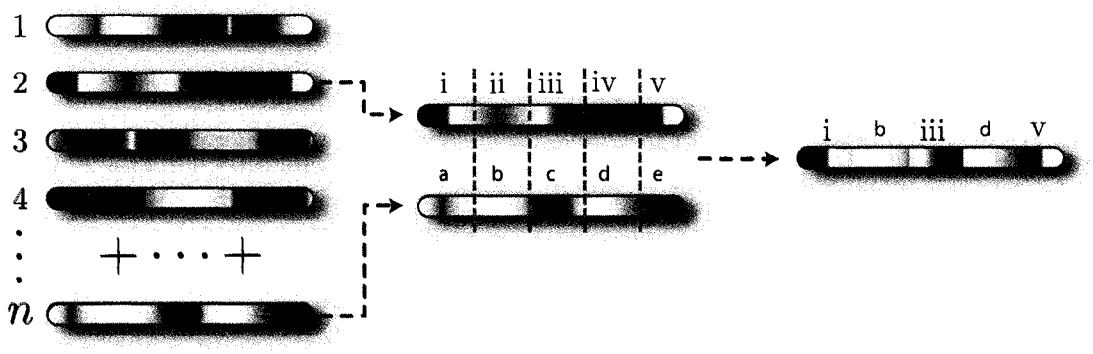

FIGURE 1.12 Schematic representation of the genetic algorithm. We start with an initial population with n individuals each composed of five chromosomes. Two fit individuals from this generation are selected and a new individual is created using a cross-over technique.

mathematical test which tells the algorithm which individuals exhibit the most favourable traits. When the fittest individuals are selected, they are used to form the next generation using genetic operations. These genetic operations can include chromosome recombinations, cross-overs, mutations, etc. The whole generation forming process is repeated until a satisfactory solution is found as per the fitness parameter. Refer to Figure 1.12 for a schematic representation of a genetic *step*.

In the case of the hydrogels used here for drug release, the chromosomes are defined as regions with a given obstacle concentration and distribution (*e.g.*, rings, grids, layers). The genetic algorithm has to find a specific arrangement of chromosomes which favours a controlled release profile. Also, mutations are introduced once a new specimen is created in order to introduce potentially beneficial changes into the population by randomly changing a certain characteristic [47]. This has been argued to help the algorithm avoid local minima by always introducing new components to the population which would otherwise tend to all look similar; effectively slowing evolution. Genetic algorithms have a tendency to get stuck in local minima unless the mutation rate and the exact implementation of the cross-overs are closely monitored. Specifics of the particular implementation of our genetic algorithm applied to hydrogels is further discussed in Chapter 2.

The use of other optimization algorithms has been considered (*e.g.*, Metropolis simulated annealing) and is discussed later. The selection step used in ranking hydrogels (*i.e.*, computing the drug release profile) which produce controlled release rates is a computationally intensive process. For this reason, the genetic algorithm lends itself well since it allows one to make significant improvements to the hydrogel for every selection step thus minimizing the need to re-evaluate the

release profile every time minor changes are made to obstacles (*i.e.*, quick scanning of the solution phase-space).

1.6 Characterization techniques

When analyzing a drug release profile, it is important to have an efficient way of characterizing its various features (*i.e.*, evaluate a specimen's fitness) in order to classify it. As discussed earlier, the analytic expression for diffusion is no longer valid as the concentration of obstacles increases. It is also not easily adaptable to various hydrogel geometries. For this reason, some have been using various functions which describe many forms of the release profiles with varying degrees of success. These empirical functions are of great experimental as well as theoretical importance since they are frequently used by many in order to compare diffusion profiles and in attempts to explain underlying phenomena [48–50].

One of the earlier characterization tool comes from Higuchi [51] and is very simple:

$$M(t) \propto \sqrt{t}\,. \tag{1.38}$$

This indicates that the fraction of released drugs is proportional to $\sqrt{t}$. This describes the "quasi-stationary" state of the effective drug front once an initial lag time has elapsed and undergoes normal Fickian diffusion. The Higuchi function has been cited in over 500 journal articles since its first appearance in 1961.

However, we concentrate our studies on two empirical functions and their ability to properly describe drug release profiles from uniformly loaded hydrogels. The first function seen here is a generalization of the Higuchi function which can be applied to drug release with combined types of diffusion. It was first used by Korsmeyer *et al.* and is known as the Peppas fit [52]. A simple power law is used to model the drug release profile:

$$\tilde{M}(t) = \frac{M(t)}{M_0} = \left(\frac{t}{t_\alpha}\right)^\alpha \tag{1.39}$$

where $\tilde{M}(t)$ is the normalized total release as a function of time, M_0 is an arbitrarily chosen normalization parameter (as defined in Eq 1.37), and α is said to be an exponent indicative of the diffusional mechanism. The initial load M_0 is a logical choice and $0 \leq \tilde{M}(t) \leq 1$ by definition; the resulting time scale t_α can then be compared to t_β for short times ($\tilde{M} \ll 1$). According to the

literature, for Fickian diffusion, $\alpha = 0.5$ and Eq 1.39 becomes similar to Eq 1.38 whereas $\alpha = 1$ would indicate Case II transport and intermediate values would be simply classified as anomalous diffusion [53]. This will be investigated and demystified in upcoming chapters. Namely, the value of α will be shown to not be reliable at all when fitting various drug release profiles! Further, since Eq 1.39 is unbounded, the fractional value of the release rate diverges starting at $t = t_\alpha$. This function cannot yield any important information about long time release and is usually only used to model drug release until $\tilde{M}(t) \simeq 0.60$. It is sometimes useful to use a piecewise variation on the Peppas function which is artificially bounded at a sufficiently large time, t_α:

$$\tilde{M}(t) = \begin{cases} \left(\frac{t}{t_\alpha}\right)^\alpha & \text{if } 0 < t < t_\alpha, \\ 1 & \text{if } t \geq t_\alpha. \end{cases} \tag{1.40}$$

By far, the most successful empirical function in characterizing drug release profiles is named after the Swedish scientist Waloddi Weibull [54]. He published a paper on the Weibull distribution in 1951, which he used to characterize strength of materials and fatigue data and for which he received much attention [55]. Incidentally, it later proved to be of great empirical importance in the field of pharmaceutics [56]. This stretched exponential function can be written as

$$\tilde{M}(t) = \frac{M(t)}{M(\infty)} = 1 - \exp\left[-\left(\frac{t}{t_\beta}\right)^\beta\right] \tag{1.41}$$

where $M(\infty)$ represents the amount of drug that escape as $t \to \infty$ ($M_\infty \leq M_0$ since some drugs may remain trapped inside), β is the so-called release exponent, and t_β is the characteristic time for the fit. There have been some mathematical, Monte Carlo, and experimental studies of diffusion which made use of the Weibull function and exploited its various characteristics [48, 57–61]. The main advantage of the Weibull function is its ability to fit release profiles independently of the geometry of the release platform or the type of diffusion. The Weibull function fits any kind of diffusion as well as special cases of mixed diffusion (normal and anomalous). For this reason, it is frequently used in the literature as a base reference guide for comparing various drug release profiles. However, one must take note that there isn't necessarily a physical basis for using the Weibull function; it just happens to fit well. It is used throughout the literature under various forms depending on the uses. For example Lánský and Weiss use the following modified version of the Weibull function [62]:

$$\tilde{M}(t) = 1 - \exp\left[-\frac{r}{1-h}t^{1-h}\right] \tag{1.42}$$

where the parameters r and h depend on the fractional diffusion rate. In this case, the escape rate is:

$$\dot{\tilde{M}}(t) = rt^{-h}\left(1 - \tilde{M}(t)\right) . \tag{1.43}$$

These authors give the parameters some kind of kinetic meaning [62].

Many have sought to attribute deeper fundamental physical diffusion properties as a function of the value of the release exponent obtained in the fit. For example, some have proposed that specific values of β are direct evidence of certain types of diffusion [53, 62]. In upcoming chapters, we will demonstrate that the release exponent depends on time and does not reliably converge to a fixed value depending on the internal geometry of the hydrogel. We show that although the Weibull function fits any release profiles relatively well, it cannot hope to convey significant properties of the hydrogel nor the type of diffusional properties.

1.7 Presentation of the thesis

This thesis is composed of two articles submitted for publication (one pending peer review) in scientific journals during the course of my M.Sc. degree. Below is a list of these articles, with a few added notes. Some unpublished work on a novel hybrid Metropolis/Genetic algorithm optimization technique is also briefly presented since some of the results may be of interest to the reader. Also note that the references are found in Chapter 6 except for those contained in the following two article/chapters.

1) S Casault, M Kenward, and GW Slater. *Combinatorial design of passive drug delivery platforms* ***In press with the International Journal of Pharmaceutics*** (2006).

   This article illustrates how one can control the rate of release of solute from a simulated hydrogel by carefully arranging its geometrical properties. This proof of principle study uses a three pronged approach to show that a controlled rate of release can be obtained. We have implemented a method to obtain the exact release profile from any given hydrogel configuration; a method to quickly generate a large number of varying hydrogel structures; and a genetic optimization algorithm which leads to the selection of optimal structures. In this article, we also rigorously test the exact enumeration method by comparing it to an analytic solution as well as various empirical functions for diffusion. I was the principal author of this paper and principal creator of the computational algorithms as well as analyzed all the data.

2) S Casault and GW Slater. *Testing the Weibull and Peppas functions in characterizing drug release profiles using an exact enumeration scheme.*

   In this article, we have carefully analyzed two empirical functions that are widely used to describe the drug release profiles. Since our method provides exact release rates, we can analyze release profiles from hydrogels at various obstacle concentrations and geometries with a high level of accuracy. Namely, we study the Peppas and the Weibull function and their possible applications. We show that the free parameters in those two functions greatly depend on time. We conclude that one should thus use caution when comparing drug release profiles from various hydrogels by looking at parameters from either of these fits. Also, only very limited physical insights about the nature of the hydrogel or the mechanism of diffusion are given by these parameters although many attribute such qualities to them.

1.8 Other contributions

In the course of my M.Sc. studies, I presented the results of my work at various conferences and workshops in Canada and abroad. Below is a summary of these research related activities, in chronological order.

Conference presentations

1) **S Casault**, M. Kenward, and GW Slater. *Combinatorial design of passive drug delivery platforms.* AFMNet Annual Scientific Conference, Calgary, 2006.

2) **S Casault** and GW Slater. *A combinatorial approach to controlling drug delivery from passive hydrogels.* Ottawa-Carleton Institute of Physics, Ottawa, 2005.

3) **S Casault** and GW Slater. *A combinatorial approach to controlling drug delivery from passive hydrogels.* Funct. Foods Nutraceuticals & Nat. Health Prod. Workshop, Montréal, 2005.

4) **S Casault** and GW Slater. *A combinatorial approach to controlling drug delivery from passive hydrogels.* The Atlantic HQP Summit, Halifax, 2005.

5) **S Casault** and GW Slater. *A combinatorial approach to controlling drug delivery from passive hydrogels.* AFMNet Annual Scientific Conference, Toronto, 2005.

6) **S Casault** and GW Slater. *A combinatorial approach to controlling drug delivery from passive hydrogels.* American Physical Society March Meeting, Los Angeles, 2005.

7) **S Casault** and GW Slater. *A combinatorial approach to controlling drug delivery from passive hydrogels.* Hydrogel Summit, Halifax, 2004.

2

Combinatorial design of passive drug delivery platforms

S Casault, M Kenward, and GW Slater. In press with *Int. J. Pharm.* (2007).

Combinatorial design of passive drug delivery platforms

Sébastien Casault, Martin Kenward, and Gary W. Slater
Department of Physics, University of Ottawa, 150 Louis-Pasteur, Ottawa, Ontario K1N 6N5, Canada
(Dated: March 29, 2007)

We introduce a novel computational approach to designing passive drug delivery systems based on porous materials such as hydrogels. Our approach uses three tools: a method to establish the exact release pattern from all possible loading sites inside a given hydrogel; a method to generate a large number of hydrogel structures to be tested numerically, and finally an optimization algorithm which leads to the selection of optimal hydrogel structures. Using this approach, we show that controlled release curves can be obtained by using a genetic algorithm for the optimization step. Strategies to generalize this approach to other systems are also discussed.

Keywords: Drug Delivery; Controlled Release; Hydrogels; Optimization; Genetic Algorithm; Exact-enumeration

I. INTRODUCTION

Designing drug-delivery systems with a controlled rate of drug release is crucial for applications where dosage must remain in a prescribed therapeutic range over the entire term of treatment [1]. Currently, there exists activation modulated platforms relying on kinematic effects (*e.g.* swelling and dissolution) that feature controlled release characteristics [2, 3]. However, it proves much more challenging to achieve constant drug release from passive platforms, *i.e.*, those strictly relying on diffusion as a drug delivery mechanism, such as non-degradable hydrogels [4, 5]. Passive platforms would have the advantage of not heavily relying on environmental factors which can prove difficult to control. There is a definite need for a systematic approach which can quickly identify optimal design strategies for passive systems.

According to Cohen and Erneux [6], the most common drug delivery mechanism is diffusion from a polymeric system (such as a hydrogel). We will thus focus our study on hydrophilic drugs escaping from non-swelling diffusion-controlled hydrogels. Since this is the most widely applicable release mechanism [7], several methods can be used experimentally to prepare hydrogels with specific internal structures (obstacle distributions). For example, Liang et al. [8] have shown that the density of a hydrogel can be controlled using a non-cytotoxic crosslinker.

We introduce the novel concept of combinatorial drug delivery platform design. This technique is used to investigate hydrogel structures which exhibit specific release characteristics. We focus this proof of principle study on obtaining results which promote a constant drug release rate as a function of time although the technique can be used, in principle, to achieve virtually any desired release profile. The results presented in this paper are obtained using a lattice model of diffusion which is similar to that introduced originally by Majid et al. [9]. We neglect chemical details and adopt a coarse-grained view of the diffusion process. Studies which model polymers often rely on stochastic, Monte Carlo simulation methods where the diffusion of a drug molecule is represented by random, discrete jumps on a lattice occupied with obstacles. In contrast, our method has the advantage of producing numerically exact data by enumerating all possible walks on any given lattice matrix with obstacles (the latter represent the gel fibers present in a hydrogel matrix). We limit our work to diffusion in two-dimensions but the extension to 3D (or more!) poses no difficulty other than requiring more computational resources.

It is widely known that the internal structure of a hydrogel is important in modulating the release rate [10–14]. Constructing hydrogels with specific structures and testing their drug release properties is experimentally time consuming. Using our method, we can reduce the amount of experiments needed by offering critical information on how to tailor the structure of a hydrogel in order to obtain specific release profiles. Although the structure of the hydrogel is important, the initial loading of the drug itself inside the structure is equally critical. Accordingly, we will also use our optimization technique to investigate the placement of drug reservoirs inside the hydrogel.

It is also possible to obtain numerically exact values of the diffusion coefficient for practically any hydrogel structure [15–17]. However, the diffusion coefficient is not always the key factor in predicting the release characteristics of complex systems (*e.g.*, one must also consider the geometry and dimensionality of the hydrogel). For this reason, we use the exact enumeration model mentioned earlier which makes no assumption about the functional form of the diffusion coefficient. This numerically exact lattice calculation of the short-time diffusion dynamics of a particle is much quicker to perform than Monte Carlo simulations. This method essentially consists in finding the transfer matrix for any given obstacle configuration and their relative positions as a function of time. Thus, any minor change to either will equate to changing a single row in the transfer matrix and thus can be recomputed fairly easily. This allows one to very quickly perform changes in the initial conditions (e.g., modifying the obstacle pattern) and measure the resulting escape rates. Using a genetic algorithm as our optimization tool, it is then possible to study several thousand combinations of (evolving) hydrogel structures in order to rank them ac-

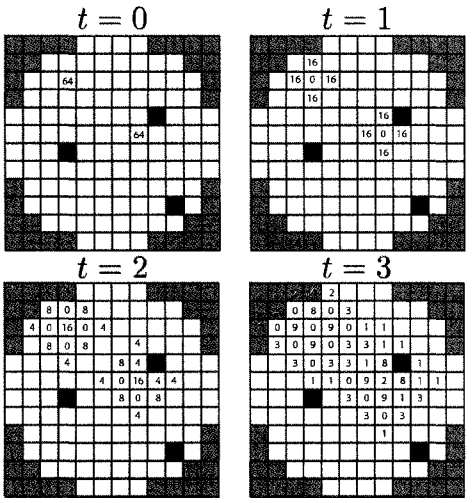

FIG. 1: Time evolution of a typical circular system with particles undergoing diffusion on a 2D square matrix with three obstacles (black). The absorbing boundary is shown in grey (the sides are also part of this boundary). The initial configuration is shown at $t = 0$ with the drug molecules completely localized on two sites.

cording to their usefulness in generating desired release rates.

This article is structured as follows: we begin by presenting the theory of the enumeration method followed by examples to test its validity. The optimization technique used throughout this paper is then presented. Finally, we present results obtained using our technique for drug delivery systems with different geometries.

II. ENUMERATION METHODOLOGY

A. Diffusion model

Enumeration methods allow one to obtain exact numerical results for problems related to diffusion, escape rates and transient effects [9]. To illustrate this, let us first examine diffusion on a simple 2D square lattice (figure 1). We compute all possible particle trajectories of a solute, based on its initial location and its probability to diffuse to any first nearest neighbour on the lattice. Figure 1 shows the evolution through 3 time steps of solute diffusion on a typical 2D square lattice with 3 obstacles.

The probability to diffuse in any given Cartesian direction is simply $p_{\pm x} = p_{\pm y} = 1/4$. In an isotropic system, a given solute particle has an equal probability to diffuse (or jump) to any four of the nearest neighbour sites. Time is discrete and all particles must attempt a jump at each time step. A move is simply rejected (*i.e.*, the particle is reflected) if the neighbouring site is occupied by an obstacle. In other words, we assume elastic collisions. Lattices with higher coordination numbers such as the hexagonal lattice were considered for this model; however they lead to prohibitively long computational times and marginal differences in release profiles.

A uniform probability of jumping is valid as long as there is no drug-hydrogel affinity, external field or other source of anisotropy. For example, in a real system the drug may exhibit affinity for the obstacles. This could be implemented by adding a probability p_o for the particle to stay on the same site when it is next to a "sticky" obstacle.

In the current study, obstacles are completely passive and do not respond to temperature variations or external effects (varying pH, electric fields, etc.). Also, the obstacle density is time-independent, *i.e.*, there are no degradation or swelling effects. Such active parameters would require major changes to the method introduced in this article since they generally involve a non-deterministic evolution of the hydrogel matrix.

The general two-dimensional master equation governing the probability of having a drug concentration $C_{x,y}(t)$ on a free site at (x, y) at time t is:

$$\begin{aligned} C_{x,y}(t+1) &= [C_{x-1,y}(t)(1-q_{x-1,y}) + C_{x,y}(t)q_{x+1,y}]\,p_{+x} \\ &+ [C_{x+1,y}(t)(1-q_{x+1,y}) + C_{x,y}(t)q_{x-1,y}]\,p_{-x} \\ &+ [C_{x,y-1}(t)(1-q_{x,y-1}) + C_{x,y}(t)q_{x,y+1}]\,p_{+y} \\ &+ [C_{x,y+1}(t)(1-q_{x,y+1}) + C_{x,y}(t)q_{x,y-1}]\,p_{-y}. \end{aligned} \tag{1}$$

In this equation, $q_{x,y}$ is the site occupation index; its value is 1 if the site at (x, y) is occupied by an obstacle and 0 if not. Note that for a given system, the value of $q_{x,y}$ is fixed for all lattice sites and is simply determined by the structure of the hydrogel. As schematically illustrated in figure 1, the calculation is done iteratively, from an initial drug concentration $C_{x,y}(0)$ for each site on the lattice. We make the assumption that we are in the low drug concentration (dilute) regime where solute particles do not interact with each other.

In order to model drug release from a finite-sized hydrogel system, one simply imposes absorbing boundary conditions $p_{\pm x} = p_{\pm y} = 0$ on the outer boundary of the hydrogel structure. The amount of drug crossing this boundary is the cumulative sum of all those probabilities which have crossed the boundary up to time t.

In this paper we restrict our work to examine simple cases which do not include surface kinetic effects. Nevertheless it is straightforward to tailor the surface properties of our simulated drug delivery system to reflect conditions which may arise from certain hydrogel/solute/environment configurations (e.g., resistance to escape at the boundary, pH or viscosity gradients at the surface of the hydrogel, etc).

If the various local concentrations $C_{x,y}(t)$ (including those in the absorbing layer) are grouped into a column vector $|C(t)\rangle$ with s elements (one for each lattice site;

note that we use Dirac's bra-ket notation), equation 1 can be rewritten as a matrix equation

$$|C(t+1)\rangle = \mathbf{T}|C(t)\rangle. \tag{2}$$

The $s \times s$ Markovian matrix $\mathbf{T}$ (which depends entirely on the positions of the obstacles) transforms the distribution at time t into the one at time $t+1$. This provides a simple computational method to carry out the iterations that are implicit in equation 1 starting from an initial drug load $|C(0)\rangle$. Mathematically, it is possible to use this equation backwards, *i.e.*, start with a given final release rate and calculate the corresponding initial configuration. This unfortunately yields unrealistic parameters (e.g. negative initial concentrations in certain regions) and is not useful in practice.

Using this exact enumeration method, we calculate the associated release rate curves. Our goal is to find an initial capsule configuration (which is defined by the obstacle locations $\mathbf{T}$ and drug loading $|C(0)\rangle$) which yields a desired release rate, e.g., a constant release rate for long time periods.

B. Notation

For the sake of clarity, we introduce the notation $M(t)$ to indicate the total drug released as a function of time:

$$M(t) = M_0 - \int_0^t \int_\Omega C(\vec{r}, t')\mathrm{d}\Omega\mathrm{d}t' \tag{3}$$

where

$$M_0 = \int_\Omega C(\vec{r}, 0)\mathrm{d}\Omega \tag{4}$$

represents the total initial amount of drugs present in a hydrogel. $C(\vec{r}, t')$ describes the drug concentration at position $\vec{r}$ at time t' and Ω represents the area (or volume for three-dimensional simulations) of the hydrogel. One can write $\tilde{M}(t)$ as the normalized cumulative amount of drugs released at time t

$$\tilde{M}(t) = \frac{M(t)}{M_0}\ . \tag{5}$$

One can define an asymptotic release amount $M(\infty)$ (it is equal to the M_0 if no drug particle is trapped inside the hydrogel). Also, we introduce the parameter τ_ϕ which we define as the time at which a certain fraction, ϕ, of drugs has been released from the system

$$\phi = \frac{M(\tau_\phi)}{M_0}. \tag{6}$$

Finally, the rate of drug release is measured by the derivative

$$\dot{M} = \frac{\partial M}{\partial t}. \tag{7}$$

Similarly, one can define a normalized rate $\dot{\tilde{M}}(t)$.

C. Uniformly loaded gels: Empirical fits

A uniformly loaded gel is defined as having an equal concentration of solute on every non-obstacle site; drug is said to be uniformly loaded in the hydrogel matrix. There is no lag time (*i.e.*, time lapse between the beginning of the enumeration and the arrival of the effective drug concentration "wavefront" at the boundary) in this scheme since there is a drug concentration near the boundary which escapes the hydrogel at $t = 1$. We later show that optimization of the hydrogel matrix can be related to this lag time and that schemes involving drug reservoirs that are non-adjacent to the boundary can be of crucial importance when searching for a constant rate of release.

We can simulate such a uniformly loaded hydrogel and compare our numerical data with two widely-used empirical fits. According to Peppas [18], a simple power-law relationship can describe the time dependence of drug release until 60% of the initial load has been released:

$$\tilde{M}(t) = \left(\frac{t}{t_\alpha}\right)^\alpha \tag{8}$$

where α is the release exponent, and the resulting time scale t_α is relevant only for short times ($\tilde{M} \ll 1$). Since the Peppas equation is not bounded as $t \to \infty$ it cannot be used to model the escape at long times.

According to a more general statistical theory, the Weibull model predicts that the release rate behaves like a stretched exponential [19]:

$$\tilde{M}(t) = 1 - \exp\left[-\left(\frac{t}{t_\beta}\right)^\beta\right]. \tag{9}$$

The parameters are now the exponent, β and the time scale t_β. A series expansion of the Weibull function yields the Peppas law to first order and thus it is expected that $\beta \to \alpha$, and $t_\beta \to t_\alpha$, as $t \to 0$. However, both these empirical fits suffer from an apparent lack of physical meaning associated with the free parameters.

D. Exact solution for a test system

It is possible to solve the 2D diffusion equation in polar coordinates for $C(r, t)$ to obtain a predicted release curve from a round hydrogel with radius r_0 [20] and uniform drug concentration. In this case, we simply replace the obstacles inside the capsule by an effective viscosity (or, more precisely, by an effective diffusion coefficient D^*) which models the retarded diffusive motion of the particles. Since the distribution of obstacles is assumed to be isotropic, D^* is simply a fitting parameter.

We study here a circular drug capsule with an isotropic obstacle distribution with a concentration well bellow the percolation threshold, $\mathcal{C}^*_{\mathrm{obst}}$ ($\mathcal{C}^*_{\mathrm{obst}} \simeq 0.408$ for a square

TABLE I: The first four λ values and the corresponding $C_n(r_0)$ coefficients used in the diffusion equation with $r_0 = 1$.

n	λ_n	$C_n(r_0)$
1	2.4048	1.6020
2	5.5201	-1.0648
3	8.6537	0.8514
4	11.7915	-0.7296

lattice [21]). The capsule is said to be uniformly loaded, *i.e.*, an equal drug concentration occupies every non-obstacle site. The $2D$ diffusion equation in polar coordinates can be written as

$$\frac{\partial C(r,t)}{\partial t} = D^* \left(\frac{\partial^2}{\partial r^2} + \frac{1}{r}\frac{\partial}{\partial r} \right) C(r,t) \qquad (10)$$

with boundary conditions

$$C(r,0) = \mathcal{H}(r - r_0)C_0 \qquad (11a)$$
$$C(r_0,t) = 0, \qquad (11b)$$

where $\mathcal{H}$ is the Heaviside function, and C_0 is the initial drug concentration of the free sites inside the capsule. Equation 11b accounts for the absorbing boundary. The solution to equation 10 is given by the following:

$$C(r',t) = \sum_{n=1}^{\infty} C_n(r_0) J_0(\lambda_n r') \exp\left[-D^* \left(\frac{\lambda_n}{r_0} \right)^2 t \right] \qquad (12)$$

where J_0 is the 0^{th} order Bessel function of the first kind, λ_n represents the n^{th} zero of $J_0(r)$, $r' = r/r_0$ is a scaled radial position, and the coefficients, $C_n(r_0)$, are given by:

$$C_n(r_0) = \frac{2C_0}{J_1^2(\lambda_n)} \int_0^1 \mathcal{H}(r - r_0) J_0(\lambda_n r') r' \, \mathrm{d}r'. \qquad (13)$$

Table I shows the first four $C_n(r_0)$ coefficients in the series solution to the diffusion equation. In the next two sections, we will compare our exact enumeration results to the Peppas and Weibull empirical fits as well as to this exact solution based on the existence of an effective diffusion coefficient D^* for the given system.

E. Round capsule with a periodic gel

We begin by constructing a simple periodic gel in order to compare our exact numerical results with empirical predictions and analytic results described in the previous section. We use a round 2D capsule constructed inside a 200×200 square lattice with a periodic obstacle distribution of concentration $\mathcal{C}_{\text{obst}} = 1/9$ (see figure 2). The drug was loaded uniformly inside the matrix (*i.e.*, the initial drug concentration was normalized at $C_0 = M_0/s$ for all

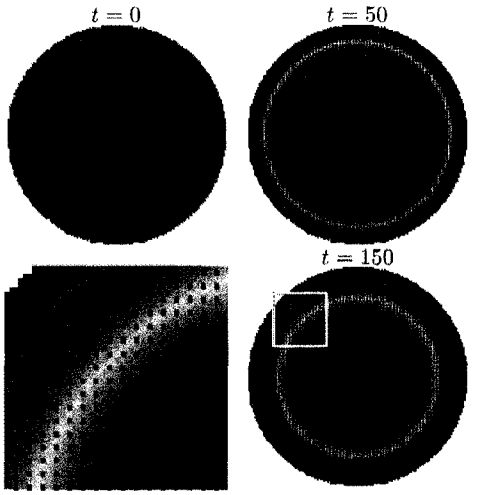

FIG. 2: Time evolution of the drug concentration inside a round drug capsule ($r_0 = 100$) with a periodic obstacle distribution ($\mathcal{C}_{\text{obst}} = 1/9$). Shown is the drug concentration from low to high concentrations (denoted by colours ranging from blue to red, respectively). The concentration of drug is uniform inside the capsule at $t = 0$. The bottom left figure is a blow up of the indicated section in the $t = 150$ figure.

sites that are not occupied by an obstacle, where s is the number of such sites). We calculate the time evolution of the population of non-interacting particles using equation 1 where t is given by the iteration step count, an integer.

The analytical function requires a value for the diffusion coefficient which we must obtain in order to compare the analytical profile with our exact numerical results. It is possible to fit the curve in order to extract the coefficient; however, there is a better way. The diffusion of a solute through an infinite lattice has been extensively studied by our group using another exact numerical approach [15, 16]. Using that technique, the scaled diffusivity for a particle in a periodic 2D square lattice of concentration $\mathcal{C}_{\text{obst}}$ was found to be given by:

$$D^* \simeq \frac{1 - \pi\mathcal{C}_{\text{obst}} + \frac{\pi^2}{2}\mathcal{C}_{\text{obst}}^2 + \cdots}{1 - \mathcal{C}_{\text{obst}}}. \qquad (14)$$

This value for D^* is then used to calculate the release profile obtained by solving equation 10. The diffusion coefficient is strictly used to compare equation 12 with results from our exact enumeration.

Figure 3 shows a plot of the release profile as a function of time as well as the three fits mentioned in the previous sections. The inset shows another view of the same data. The Weibull fit is in good agreement with our release profile up to $\tilde{M}(t) \simeq 0.9$ and the Peppas fit is valid up to $\tilde{M}(t) \simeq 0.65$. The values obtained for the

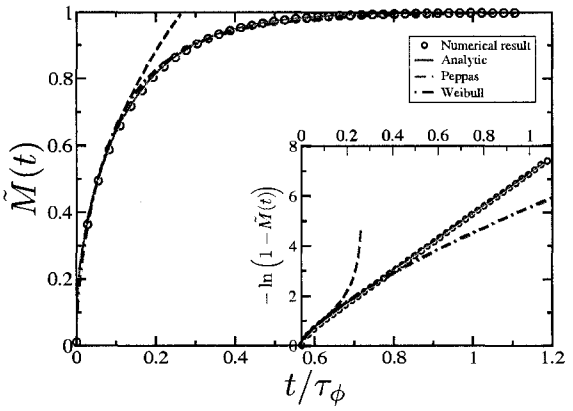

FIG. 3: Total drug release as a function of time for a round drug capsule of radius $r_0 = 100$ (see figure 2) with a periodic obstacle concentration $\mathcal{C}_{\text{obst}} = 1/9$. The parameters of the different fits are (see text for definitions): Peppas, $t_\alpha/\tau_\phi = 0.25$, $\alpha = 0.46$; Weibull, $t_\beta/\tau_\phi = 0.1$, $\beta = 0.72$, $M(\infty) = M_0$ here since there are no traps; analytic, $C_0 = 1.0$, $D^* = 0.8008$, 5 terms in the series. The value for τ_ϕ was computed using $\phi = 0.999$ and was used to transform the data from both the enumeration and the analytic solution. The curves were then fitted on this transformed graph. The inset shows very good agreement of our data with the analytical solution by using a $-\ln\left(1-\tilde{M}(t)\right)$ y-axis transformation.

fitting exponents α and β are consistent with findings made by Papadopoulou *et al.* [22] for Fickian diffusion. The value of $D^* = 0.8008$, as obtained from equation 14 for $\mathcal{C}_{\text{obst}} = 1/9$, is used to plot equation 12 in figure 3. The analytical solution is in remarkable agreement with our exact numerical results for the release rate. This indicates that periodic obstacles can indeed be replaced by a constant viscosity within the hydrogel.

This example is used as a benchmark to properly gauge the accuracy of our model. At first glance these empirical laws seem to limit our control of the release rate. However, it is important to keep in mind that they are based on idealized conditions (uniform distribution of drug and obstacles, etc.) and thus it is possible to change these characteristics and manipulate the diffusion process. In section III, we present a method for obtaining release profiles that are different from these standard release curves in order to systematically control the drug release.

F. Round capsule with a random gel

The characteristics of drug release are strongly influenced by the behaviour of drugs which linger inside the hydrogel (e.g., slowly decaying tail on the drug release curves for long times). This behaviour is affected by the obstacle configuration and density. We now study the effects of altering the obstacle properties using a round capsule constructed inside a 200×200 square. The obstacles are placed randomly inside the round matrix and the drug is distributed uniformly on the remaining empty sites. The release curves are shown in figure 4 for varying obstacle concentrations. The solid lines correspond to solutions of equation 10. Again, we can obtain the scaled diffusivity from Mercier *et al.* [15, 16] for 2D square lattices with randomly placed obstacles with concentration below percolation:

$$D^* \simeq 1 - (\pi - 1)\,\mathcal{C}_{\text{obst}} - 0.8558\mathcal{C}_{\text{obst}}^2 + \ldots. \qquad (15)$$

The resulting curves are in remarkable agreement with our enumeration results in the limit of low obstacle concentrations, $\mathcal{C}_{\text{obst}} \lesssim 20\%$.

Due to the finite sizes of our hydrogels, the drug molecules will undergo anomalous diffusion for a certain portion of the release profile (except at $\mathcal{C}_{\text{obst}} = 0$) before making a transition to normal diffusion. This is a well documented phenomenon and corresponds to a transition from anomalous diffusion to normal (or Fickian) diffusion which occurs after the molecules have travelled a certain cross-over length (or time) [9, 18, 23–26]. This cross-over length becomes larger as $\mathcal{C}_{\text{obst}}$ is increased until it is on the order of the size of our system (the cross-over length diverges at $\mathcal{C}^*_{\text{obst}}$). At this point, anomalous diffusion is observed for all times in our enumerations. Drug escapes from connected and tortuous pathways with a large number of dead ends altering the shape of the release profile [27]. Discrepancies between analytical and enumeration profiles are due to the fact that the analytical theory assumes a homogeneous diffusion coefficient throughout the hydrogel although this is not the case. Our enumeration model makes no such assumption and performs exact calculations of escape for each drug molecule from every hydrogel configuration.

There is also an increasing percentage of drugs which remain trapped inside the hydrogel as the obstacle concentration is increased. This is seen on figure 4 for release curves from hydrogels of $\mathcal{C}_{\text{obst}} \geq 0.35$. These profiles attain a plateau value which is not equal to unity. We have access to the exact number of trapped particles during an enumeration and we can set the value of M_0 to be rescaled as $M(\infty)/M_0$ in order to compare the enumeration results with the analytical solution (equation 12 is used for the solid line fits in figure 4). As seen, the analytical theory breaks down in the near percolation limit. It is also interesting to note that the drug release rate can also be higher than anticipated. This can be seen on the release profile associated with an obstacle concentration $\mathcal{C}_{\text{obst}} = 0.35$ where the initial release occurs at a faster rate than predicted by the analytical theory (see equation 4). This is due to the creation of small drug "reservoirs" near the outer surface of the hydrogel which contributes an outward biasing effect.

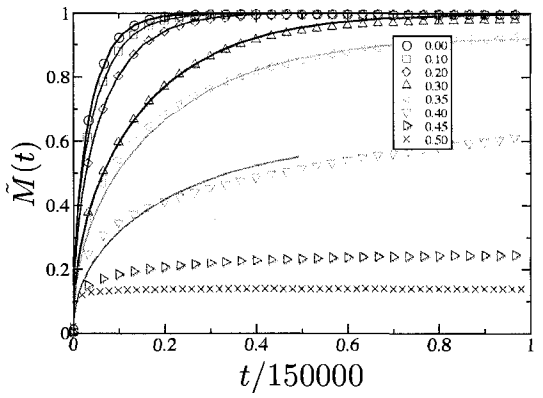

FIG. 4: Release profiles from circular random hydrogels with obstacle concentrations $\mathcal{C}_{\text{obst}}$ (shown in legend) with radius of $r_0 = 100$. There is a clear change in $\tilde{M}(t)$ as $\mathcal{C}_{\text{obst}}$ is increased. For the cases of $\mathcal{C}_{\text{obst}} = 0.35, 0.40$, $M(\infty)/M_0$ were estimated to be 0.927 and 0.612 respectively by calculating the average amount of trapped particles. The solid lines are solutions to equation 10 with values of D^* obtained from equation 15 for shown obstacle concentrations and using $M(\infty)$ as the value of the effective initial load.

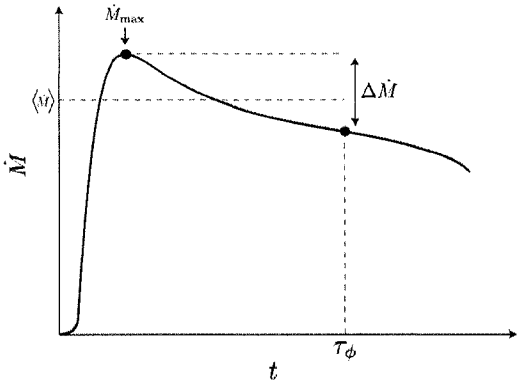

FIG. 5: Schematic illustration showing the parameters used to calculate the fitness parameter, $\mathcal{F}$, in equation 16. This is an idealized drug release rate profile, $\dot{M}(t)$.

This anomalous to normal diffusion transition has direct implications in controlling the release profile. These results suggest that high obstacle concentrations may favour slow, more constant release rate and that linear release could occur in a specific case of a power law regime (*i.e.*, case II transport [28]) of anomalous diffusion. In search of such a constant drug release profile, we will study the effects of systematically varying obstacle concentations as a function of position. We will also compare drug release profiles from hydrogels with drug loaded uniformly versus hydrogels with discrete drug reservoirs. This will be shown in section IV.

III. GENETIC OPTIMIZATION METHODOLOGY

A. Gel Structure

Determining optimal obstacle density and placement is a daunting task considering the large number of degrees of freedom, therefore we limit ourselves to the simplest experimental case and search for structures which may be tested in the laboratory. Should any symmetry or pattern be observed in the course of our optimization such as onion structures (*i.e.*, rings of varying obstacle densities), layers, or reservoirs we will use it to our advantage. Note that since we use a discretized version of the physical system and work on a 2D lattice, there is a finite number of spatial locations for the obstacles and solute particles. Finally, we restrict our examination to the low density drug limit where drug-drug interactions are negligible. In fact, there does not seem to be a significant change in the drug release profile from noninteracting particles compared to particles with hard-core excluded volume interactions [11].

B. Fitness parameter

Finding a good fitness parameter is a critical factor for any optimization process. Our algorithm needs to identify the hydrogel/drug configurations which produce a targeted release profile using a simple quantitative test. Since we are aiming to produce constant release rates (over specified time intervals) we compute the following fitness parameter (see figure 5 for schematic illustration),

$$\mathcal{F} = (1-\gamma)\Delta\dot{M} - \gamma\left\langle \dot{M} \right\rangle . \tag{16}$$

In this equation, $\Delta\dot{M} = \dot{M}_{\max} - \dot{M}(\tau_\phi)$ is the maximum value of the rate of drug release from our simulated hydrogel minus the value of the release rate at some upper time τ_ϕ (smaller values of $\Delta\dot{M}$ indicate a more constant rate of release over that period of time). $\left\langle \dot{M} \right\rangle$ is the average rate of release during this time interval. This fitness parameter thus measures the linearity of the drug release by minimizing the slope of the rate of release curve starting from its maximal peak value while increasing the average rate. The value γ is an adjustment parameter which favours either minimizing the slope or maximizing the mean release rate. Adjusting this rate permits the creation of interesting hydrogel structures which are not shown in this article (*i.e.*, γ is set to 0 except for section IV C where it is set to 0.9).

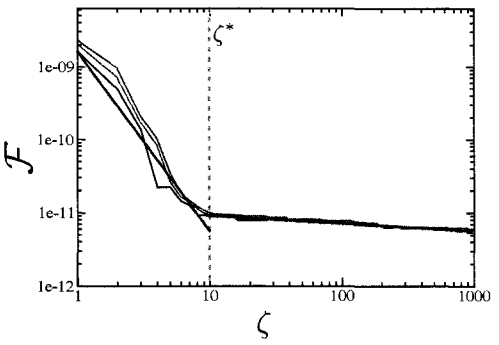

FIG. 6: Profiles of the fitness parameter, $\mathcal{F}$, as a function of generation number, ζ, for the three best candidates during a genetic algorithm optimization. We use the system discussed in section IV B for this demonstration although the general behaviour is similar for any system. The power law fits for the two regions are shown in grey and ζ^* in dashed grey. This type of data is a useful guide to gauge the required number of generations needed to attain sufficient convergence.

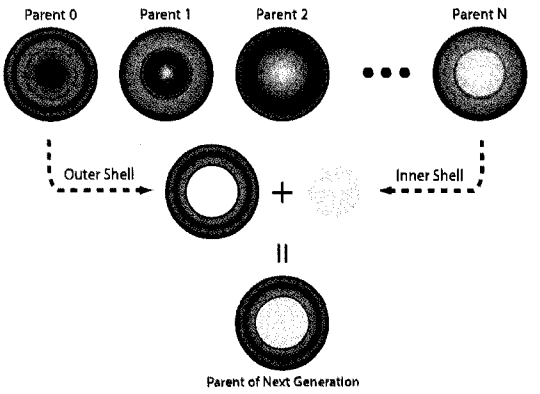

FIG. 7: Schematic illustration of a two ring cross-over from two randomly selected good parents to form an offspring in the next generation. The darker regions indicate higher concentrations of obstacles.

It is important to note that an inherent lag time often exists at the beginning of the release process which must be neglected in order to obtain our fit (see figure 5). This lag time is a transient effect due to the arrival of the effective drug "wave front" and it is related to the geometry of the system [29]. This explains why we strictly look at the "post-peak" release process.

Our algorithm begins by initializing our first generation and calculating the fitness parameter, $\mathcal{F}$, for each individual. Each generation is built using genetic characteristics from the best parents of the previous generation following the rules of the algorithm outlined in section III C. In principle, it is possible to select an appropriate fitness parameter in order to achieve any desired functional form for the release profile, $M(t)$.

As an example consider a circular random hydrogel constructed inside a 100×100 square matrix. Fitness parameter data were obtained from the simulation perfomed in section IV B. Further details on the specifics used to implement the genetic algorithm are given therein. This system serves as our typical example here. Figure 6 shows that our fitness parameter converges with increasing numbers of generations. The fitness parameter, $\mathcal{F}$, is shown as a function of the generation number (ζ) for the three best candidates. In this example, the fitness parameter decreases sharply as a function of ζ until a cutoff generation $\zeta^* \simeq 10$. This has an important significance when determining the optimal number of generations needed to equilibrate each system. The fitness parameter decreases roughly as a power law for the region $\zeta < 10$ region: $\mathcal{F} \simeq 1.6 \times 10^{-9}\zeta^{-2.5}$. For $\zeta \geq 10$, the fitness parameter approximately behaves like: $\mathcal{F} \simeq 1.2 \times 10^{-11}\zeta^{-0.1}$ (shown in grey on the figure). This system has minimized the value of the fitness parameter very quickly at low values of ζ^*. Other systems usually follow a similar trend although they generally have higher values for ζ^*.

Figure 6 also illustrates the learning mechanism of the algorithm. It shows various instances where a candidate acquires a favourable trait (*i.e.*, sudden drop in effective fitness parameter) and passes those genetic characteristics to all others within a few generations.

C. Optimizing the initial obstacle distribution

We study the effects of "intelligently" placed obstacles and drug reservoirs using an extended Compact Genetic Algorithm (eCGA)[30]. Genetic algorithms are able to quickly scan a large portion of phase space (*i.e.*, the space of obstacle and drug placement locations) and thus efficiently find a minimum. They are a class of optimization algorithms which progress by acquiring successful traits from previous generations in order to quickly converge to a solution. In our case, an ensemble of drug capsules is first initialized based on a given basic design (e.g., an onion-like layering or chessboard pattern). Each drug capsule is then assigned a fitness parameter, $\mathcal{F}$ (see section III B for details). This parameter allows one to rank the capsules according to their ability to produce the desired output (e.g., a constant rate of escape). The entire ensemble (first generation) is then analyzed and ranked according to the fitness parameter. Once the best hydrogels are found, usually 10% are kept for the next generation (elitism) and a new generation of offspring is created using specific characteristics inherited from these "parents".

We use three genetic mechanisms to construct our subsequent generations (there are many more genetic mechanisms but these will suffice for our proof of principle study). First, using a crossover technique, we take the configuration of a predetermined section (e.g., ring-like structure) of a randomly selected parent and couple this with various other (ring-like) sections from other randomly selected parents. We combine these traits to generate the next generation (figure 7 illustrates such a crossover for a circular drug capsule comprised of two rings). The second technique involves another type of crossover where a mother and a father each donate randomly selected parts of their configurations in a chessboard pattern to form unique offsprings. The former technique is useful for configurations that exhibit angular symmetry and the latter for those with Cartesian symmetry.

Thirdly, once a generation is formed, a certain percentage of mutations are introduced in these offsprings. There are three possible types of mutation. The algorithm randomly changes an obstacle for a void, it can create an obstacle from a void and it can also change the location of an obstacle (the relative probability for the mutation to be of one type is: 25%, 25%, and 50%, respectively). These mutations lead to a more thorough "scanning" of the phase-space by introducing configurations that may not be obtained through simple genetic recombinations.

The resulting offsprings are then ranked according to our fitness test and the entire process is repeated until a satisfactory candidate is found. As a caveat, note that although genetic algorithms are very efficient at locating local minima in phase space there is no way to tell if we have reached the global minimum. In our simulations, we try to minimize the chance of being trapped in a local minimum by using a large number of generations and a relatively large percentage of mutations ($\geqslant 2\%$ per generation).

D. Optimizing the initial drug reservoir position

The position and number of drug reservoir(s) may also need to be optimized in order to achieve our desired release rates. For example, in section IV C, the drug matrix is divided into a chessboard pattern, some sections of the capsule would then be given a probability of being a drug reservoir. The algorithm is free to optimally alter the number and placement of drug reservoirs within the matrix.

E. Computational details

Most of the computational work was performed on 15 dual-core UltraSPARC IV+ processors with 576GB of shared memory (www.hpcvl.org). Each simulation is executed over an average of 12 hours (depending on the size of the matrix, the total Monte Carlo time required to obtain sufficient drug release, and the number of generations). Individual analysis and smaller simulations not requiring combinatorial optimization is performed on a 3.2 GHz P4 processor with 2GB of memory.

IV. RESULTS

A. Spherical geometry with continuous drug distribution

The genetic algorithm is initially applied to a uniformly loaded circular random hydrogel constructed inside a 100×100 square lattice with radius $r_0 = 50$. The optimization is performed on the release profile from the moment that $\dot{M}(t)$ reaches its maximal value (this occurs at $t = 1$ since the hydrogel is uniformly loaded and there is no lag time in the drug release) until $\phi = 0.50$ and the adjustment parameter, γ, is set to 0. There are 1000 genetic generations and each generation is composed of 300 specimen.

Each hydrogel capsule is divided into 5 rings of equal thickness. The genetic algorithm creates new capsules using rings from 5 fit parents in the previous generation and randomly combines them as discussed earlier. Once a new hydrogel is created, mutations are introduced on 2% of the sites using the previously discussed mutation scheme.

The obstacle configuration of the optimized hydrogel can be seen on figure 8a. The associated obstacle concentration as a function of radial position, r, can be seen in figure 8c. By carefully observing figures 8a and 8b, one can notice the formation of a solid obstacle boundary (or membrane) at $r \simeq 45$ except for one small hole visible in the third quadrant of the circle. This boundary was created by the genetic algorithm in order to curtail the initial large release rate due to the bulk of the drugs' location near the surface of the hydrogel. The hydrogel has been divided into two sections with different obstacle concentrations: $\mathcal{C}_{\text{obst}} = 0.05$ in the first region while the second region has an increasing obstacle concentration. On average for the whole capsule, $\mathcal{C}_{\text{obst}} = 0.10$. Another feature of interest is that the centre of the hydrogel was chosen to contain very few obstacles (conversely, a large drug concentration). This would seem to minimize the overall impact of the initial release rate peak associated with the high drug concentration near the outer boundary of the hydrogel by locating the bulk of the drug in the centre. The ideal hydrogel seems to be one which tends to push the membrane closer to the surface of the hydrogel. By systematically increasing the value of ζ (the number of generations), one can see that it is pushed towards the outer boundary (not shown).

Figure 9 shows the cumulative release as a function of time for our optimized hydrogel (solid line) as well as a comparison with a hydrogel of uniform obstacle concentration $\mathcal{C}_{\text{obst}} = 0.10$ (dashed line). Since drugs initially occupy every non obstacle site, drugs begin escaping the

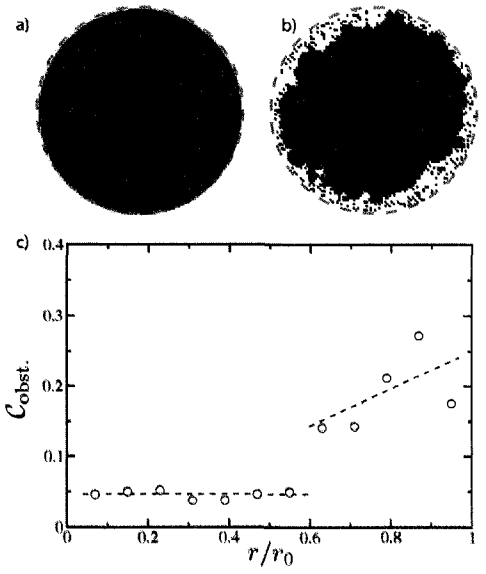

FIG. 8: a) Optimal initial ($t = 0$) hydrogel configuration of a $r_0 = 50$ capsule; obstacles are in black. The dashed grey line represents the outer boundary of the hydrogel. b) Retarding effect of the high obstacle concentration on the diffusion at $t = 1000$. There is also a very interesting visible feature – namely the formation of an obstacle barrier near the outer boundary of the hydrogel. The associated radial obstacle concentration profile is also shown in c). The hydrogel has been separated into two distinct regions. The first region $0 < r < 0.6r_0$ has a very low obstacle concentration of $\mathcal{C}_{\rm obst} = 0.05$ and the second region has an increasing obstacle concentration.

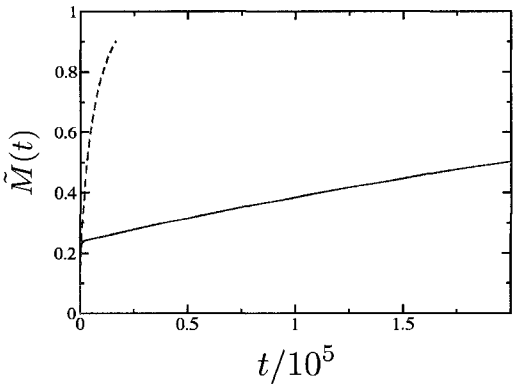

FIG. 9: Profiles of cumulative drug release as a function of time for the drug capsule shown in figure 8. This enumeration is performed until $\phi = 0.5$. There are 1000 genetic generations and each generation includes 300 specimen with a mutation percentage of 2%. The release is also compared to a control hydrogel with a uniform obstacle distribution equal to the average value of our optimized structure, $\mathcal{C}_{\rm obst} = 0.10$ (dashed line). The optimized release profile has two distinct regions. A quick initial release of drugs near the outer boundary followed by a linear release of drugs enclosed within the created obstacle boundary (porous membrane).

hydrogel as early as $t = 1$. This explains the steep initial slope observed for both hydrogels. However, once the drugs outside the bounded area observed in figure 8b have escaped, $M(t)$ in nearly lineary until $\phi \simeq 0.50$.

The circular geometry discussed in this section is a good demonstration of the usefulness of our genetic algorithm in optimizing drug release profiles. The genetic algorithm is able to find an optimized structure which produces a remarkably constant rate of release. The creation of the obstacle barrier seems to be a key component in controlling the release profile. This single hole membrane model has been extensively used in the past to obtain a constant drug release rate [31]. It is quite interesting to note that the genetic algorithm was able to form a similar structure with no prior assumptions. The optimization appears to eliminate drugs from the boundary at the same time as creating this barrier. It would be logical to further test these hypotheses.

B. Spherical geometry with central reservoir

We re-examine the drug capsule geometry used in the previous section. However, the drug will now be initialized in a single central reservoir of radius $r = 10$. The single reservoir will curtail the effects of the strong initial drug release rate observed previously. The round capsule is constructed inside a 100×100 square with drugs evenly distributed in the reservoir. For the first generation, we initialize the drug capsule with 5 rings. Each ring has a width of 10 matrix sites with randomly chosen obstacle concentrations $\mathcal{C}_{\rm obst}$ (each below the 2D percolation threshold). Our genetic algorithm is then applied.

There are a total of 1000 generations each one of which is composed of 300 specimen. Each specimen is simulated for a maximum of 200000 time steps. Each generation is constructed using the first genetic technique discussed in section III C using a simple five ring swap (*i.e.*, five chromosomes involved in the genetic optimization step) between five parents. Mutations are introduced after the crossover at a rate of 2%.

The genetic algorithm is programmed to find the configuration of obstacles which would produce the most constant release rate in a specified range of drug release (from $\dot{M}_{\rm max}$ up to $\phi = 0.50$ and $\gamma = 0$ here as well). The upper bound, $\phi = 0.50$ was chosen to be sufficiently high to control the bulk of the release profile without worrying

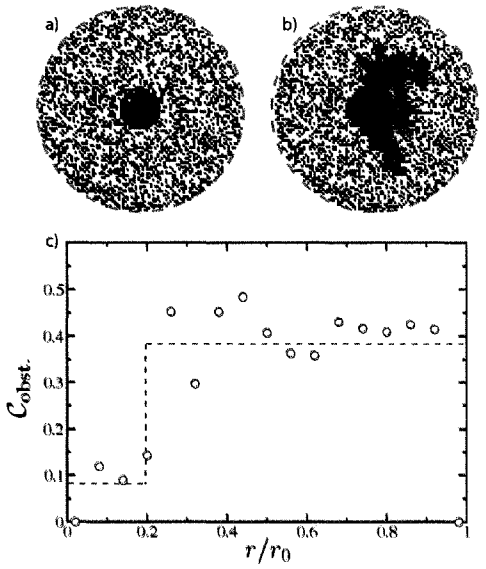

FIG. 10: a) Optimal hydrogel configuration of a $r_0 = 50$ capsule (drug reservoir in red), obstacles in black and free space in white. The dashed grey line represents the outer boundary of the hydrogel. b) Shows the retarding effect of the obstacles on the diffusion at $t = 5000$. The associated obstacle concentration profile is also shown in c). The average obstacle concentration is indicated for two regions of the hydrogel. The reservoir with a width of 10 matrix sites has $\mathcal{C}_{\rm obst} = 0.08$ whereas the rest of the hydrogel is fairly uniform with $\mathcal{C}_{\rm obst} = 0.38$. The overall obstacle concentration is $\mathcal{C}_{\rm obst} = 0.32$.

about the tailing effect.

The resulting optimal configuration is shown in figure 10a. Figure 10b shows the concentration of drugs in the hydrogel at $t = 5000$. The obstacle concentration profile has been divided into two sections (see figure 10c). The first section has a very low obstacle concentration of $\mathcal{C}_{\rm obst} = 0.08$ since it includes the drug reservoir (obstacles are allowed to enter the reservoir during genetic mutations). The second section has an average obstacle concentration of $\mathcal{C}_{\rm obst} = 0.38$ nearly at the percolation threshold. This section is suspected to be mainly responsible for having altered the shape of our release curve through the creation of another slow leaking membrane. The overall obstacle concentration is $\mathcal{C}_{\rm obst} = 0.32$. At least one ring with very high obstacle density has been observed in all specimens with this geometry and would appear to be a necessity to achieve controlled release rates.

Figure 11 shows the escape rate and the cummulative amount of drug released as a function of time. The dashed line shows a comparison of our optimized results with a hydrogel of uniform obstacle concentration $\mathcal{C}_{\rm obst} = 0.32$ equal to the average obstacle concentration

10

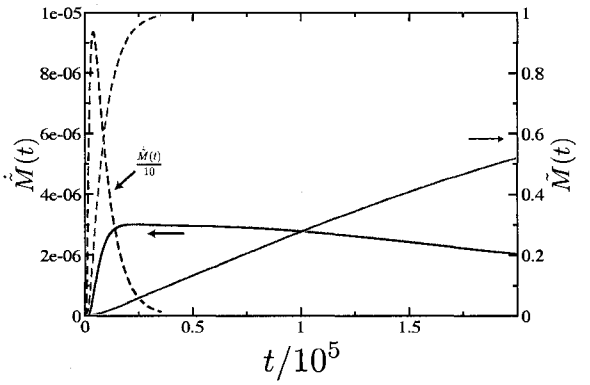

FIG. 11: Profiles of release rate, $\dot{M}(t)$, in black and total amount of released drugs as a function of time in red for the drug capsule shown in figure 10. This enumeration is performed until $\phi = 0.50$. There are 1000 genetic generations and each generation includes 300 specimens with a mutation percentage of 2%. The total release is also compared to a control hydrogel with isotropic obstacle distribution, $\mathcal{C}_{\rm obst} = 0.32$ (dashed line). The curve obtained from the comparison hydrogel was divided by 10.

of our optimal structure (the rate curve was divided by 10 in order to compare its shape). The comparison hydrogel also has a central drug resevoir of radius $r_0 = 10$.

The release profile has been improved in terms of linearity from the one observed in our standard (dashed line). It is possible to quantify this by looking at the fitness parameters. Our standard has a fitness parameter $\mathcal{F} = -2.9 \times 10^{-9}$. However, our optimal structure produces a much more constant release rate with $\mathcal{F} = -5.4 \times 10^{-12}$. This optimization can be seen on the release rate curves (black). The optimized hydrogel shows a more constant release rate since the initial peak is less pronounced and the decay is much slower than the release rate from the standard.

It is quite remarkable that we are able to significantly alter the release profile by simply reorganizing the obstacle distribution around a central drug reservoir. This could lead to the development of spherical hydrogel matrices which produce a controlled drug release rate.

C. Planar geometry with optimized reservoir distribution

We now examine a rectangular drug capsule which can be representative of a transdermal drug delivery system [32, 33]. The 2D system presented here can be seen as a cross-sectional slice of such a system. This transdermal-type hydrogel allows us to use periodic boundary conditions: where drug particles leaving the system to the

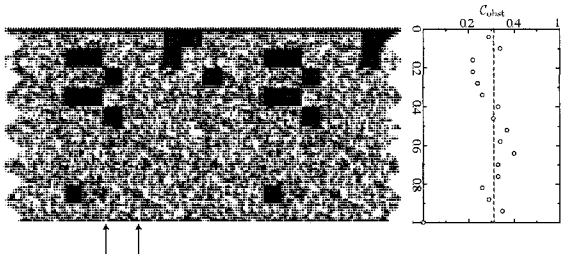

FIG. 12: Optimal drug delivery configuration of a 100×100 capsule with drug reservoirs in red, obstacles in black, and free space in white. Each drug reservoir is numbered and its contribution to the total release is shown on figure 13. There is a solid layer of obstacles on the top and bottom boundaries except for holes from which drugs can escape on the bottom (indicated by arrows in the unit cell). The obstacle concentration is shown to be quite constant inside the matrix ($C_{\text{obst}} \simeq 0.32$).

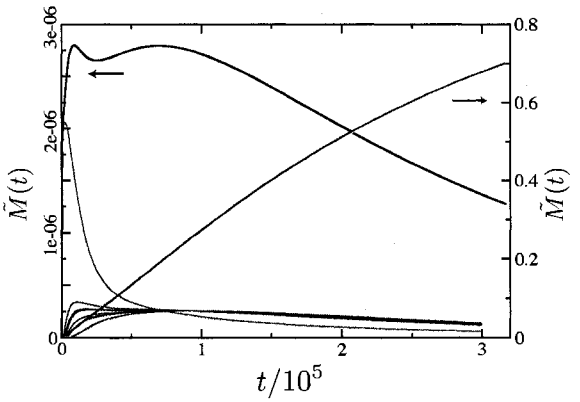

FIG. 13: Profiles of release rate (black) and total released drugs (red) as a function of time for the drug capsule shown in figure 12. This simulation ran for 3.3×10^5 time steps. There were 500 genetic generations and each generation comprised of 300 specimen. The genetic algorithm optimized the release profile up to $\phi = 0.5$. The contribution to the release rate by individual reservoirs is also shown in grey.

right are re-introduced on the left and vice versa. The unit cell of our periodic matrix measures 100×100 lattice sites and is now divided into grids measuring 10×10 sites. Each grid is initially given an obstacle concentration. We also allow the algorithm to choose the position and number of drug reservoir(s) in order to better control the drug release. The algorithm has a 20% chance of transforming a 10×10 obstacle grid into a drug reservoir during the initial creation of the hydrogel, $\zeta = 1$. These grids are now the chromosomes to be used by the eCGA.

We have incorporated the general trends observed in the previous sections directly into the initial conditions of our hydrogel in order to augment the efficiency of our optimization algorithm. In an attempt to reproduce the high obstacle concentration near the exit boundary, the lower boundary has been blocked with obstacles with the exception of 10 periodically-placed holes in the unit cell. Note that during genetic mutations, these holes are free to change location or become blocked. The eCGA can now concentrate on finding optimal obstacle structures without having to invest reorganizing steps to form the previously observed high density layer of obstacles near the boundary.

This scheme allows for the optimization of both the obstacles and the placement of the drug reservoirs. The grid pattern allows for a greater number of chromosomes used in the optimization compared to the previous section. The eCGA also uses all three genetic recombination techniques discussed in section III C. Each capsule is allowed to diffuse for 2×10^5 time steps. There are 500 generations, each with 300 specimens and a mutation rate of 2%. The genetic algorithm optimizes the release profile up to $\phi = 0.5$ and here $\gamma = 0.9$.

The optimized hydrogel slice can be seen in figure 12. The unit cell is periodically repeated on both sides for illustrative purposes. It exhibits a number of interesting features. The obstacle concentration is fairly constant and near percolation throughout the drug matrix ($C_{\text{obst}} \simeq 0.32$). Remarkably, the eCGA has obstructed all of the holes on the boundary line (shown in green) except for two which were left open for drug release. Also, the density of drug reservoirs at each grid layer is increasing as the distance from the boundary increases.

Results obtained from this matrix are shown in figure 13. The drug release rate is rather linear for the range where 5% and 60% of the drug has escaped. Controlled release has therefore been obtained by adjusting the placement of obstacles and the initial position of drug.

Since our drug particles are non-interacting, we are able to perform the simulation one reservoir at a time. This allows us to investigate the contribution to the total release from each reservoir. Figure 13 shows the contribution of each reservoir to the total release curve (grey). The total release rate from this matrix is shown in black. The total release due to all the reservoirs is shown as the red curve.

These results are quite remarkable and testify to the power of this combinatorial approach. It is clear that controlled release can be achieved using our method and that it is a matter of carefully organizing the drug matrix itself. The algorithm finds a simple structure which consists of a concentration of obstacles near percolation and a carefully placed drug pyramid-like drug placement which yields a constant release rate. A similar structure could be implemented experimentally (at least qualitatively) to serve as the basis for a constant release drug

platform.

V. CONCLUSION

In this article we propose an exact enumeration model for drug diffusion which produces results that are in agreement with empirical fits and analytical data. Using this model, we can optimize the initial conditions of a given drug matrix in order to control the rate of drug release using a genetic algorithm. We use a simple fitting parameter in order to rank drug matrices according to their ability to produce our desired rate of release.

Each structure studied allowed us to gain valuable information pertaining to the behaviour of the release profile. We first showed that it is possible to favorably alter the release profile for the simple case of a round drug matrix with a central drug reservoir.

We can also control the release rate by using a rectangular transdermal-type drug matrix with horizontal periodic conditions. It is possible to control drug release by letting the eCGA optimize the location and number of drug reservoirs. The resulting matrix from this eCGA optimization was then used to show that it is possible to re-create a constant rate of drug release by changing the position and number of drug reservoirs of the system. This allowed us to show the general characteristics drug matrices should have in order to produce a controlled rate of release.

To summarize we have demonstrated using a proof of principle study that we can systematically study the effects of drug matrix geometry on the behaviour of drug release. By beginning with a simple geometry with no immediately apparent structure and progressively varying the degrees of freedom of the system we were able to control the rate of drug release from our capsules. In particular we have shown that we can obtain an increasingly linear release rate in a reproducible manner with particular geometries that can provide impetus for the design of future drug delivery systems. The new optimization method introduced in this article can in principle be used for a wide range of drug delivery challenges.

Acknowledgments

The authors would like to thank M. Bertrand, E. C. J Oliver, and F. Tessier for useful discussions. Computational analysis was supported by the High Performance Computing Virtual Laboratory (HPCVL). This work was financially supported by research grants from the Advanced Foods and Materials Network (AFMNet) and by the Natural Sciences and Engineering Research Council of Canada (NSERC) to GWS.

[1] N. A. Peppas and R. Langer, Science **263**, 1715 (1994).
[2] S. Mallapragada, P. Colombo, and N. Peppas, J. Biomed. Mater. Res. **36**, 125 (1997).
[3] W. M. Saltzman and W. L. Olbricht, Nature Reviews **1**, 177 (2002).
[4] O. M. Conaghey, J. Corish, and O. I. Corrigan, Int. J. Pharm. **170**, 215 (1998).
[5] X. Liu, K. Nakamura, and A. M. Lowman, Soft Materials **1**, 393 (2003).
[6] D. S. Cohen and T. Erneux, SIAM J. Appl. Math. **58**, 1193 (1998).
[7] C.-C. Lin and A. T. Metters, Adv. Drug. Del. Rev. **58**, 1379 (2006).
[8] H.-C. Liang, W.-H. Chang, H.-F. Liang, M.-H. Lee, and H.-W. Sung, J. Appl. Poly. Sci. **91**, 4017 (2003).
[9] I. Majid, D. Ben-Avraham, S. Havlin, and H. E. Stanley, Phys. Rev. B **30**, 1626 (1984).
[10] B. Amsden, Macromolecules **31**, 8382 (1998).
[11] A. Bunde, S. Havlin, R. Nossal, H. Stanley, and G. Weiss, J. Chem. Phys. **83**, 5909 (1985).
[12] J. E. Hastedt and J. L. Wright, Pharm. Res. **7**, 893 (1990).
[13] K. Kosmidis, P. Argyrakis, and P. Macheras, J. Chem. Phys. **119**, 6373 (2003).
[14] J. Siepmann and N. A. Peppas, Adv. Drug Del. Rev. **48**, 139 (2001).
[15] J.-F. Mercier and G. W. Slater, J. Chem. Phys. **110**, 6050 (1999).
[16] J.-F. Mercier and G. W. Slater, J. Chem. Phys. **110**, 6057 (1999).
[17] T. M. Nieuwenhuizen, P. F. J. van Velthoven, and M. H. Ernst, Phys. Rev. Lett. **57**, 2477 (1986).
[18] N. A. Peppas, Pharm. Acta Helv. **60**, 110 (1985).
[19] W. Weibull, J. Appl. Mech. **18**, 293 (1951).
[20] J. Crank, *The Mathematics of Diffusion, 2nd edition* (Oxford: Clarendon Press, 1975).
[21] P. J. Reynolds, H. E. Stanley, and W. Klein, Phys. Rev. B **21**, 1223 (1980).
[22] V. Papadopoulou, K. Kosmidis, M. Vlachou, and P. Macheras, Int. J. Pharm. **309**, 44 (2006).
[23] J. Bonny and H. Leuenberger, Pharm. Acta Helv. **68**, 25 (1993).
[24] P. Chelminiak, R. E. Marsh, and J. A. Tuszuński, Phys. Rev. E **72**, 031903 (2005).
[25] S. Havlin and D. Ben-Avraham, Adv. Phys. **51**, 187 (2002).
[26] M. J. Saxton, Biophys. J. **66**, 394 (1994).
[27] D. Stauffer and A. Aharony, *Introduction to Percolation Theory* (Taylor & Francis, 1992).
[28] D. J. Enscore, H. B. Hopfenberg, and V. T. Stannett, Polymer **18**, 793 (1977).
[29] R. M. Barrer, J. Phys. Chem. **57**, 35 (1953).
[30] K. Sastry and G. Xiao, IlliGAL Report **2001016**, 1 (2001).
[31] R. Langer, Nature **392**, 5 (1998).
[32] R. Langer, Adv. Drug Del. Rev. **56**, 557 (2004).
[33] B. J. Thomas and B. C. Finnin, Drug Discov. Today **9**, 697 (2004).

3

Testing the Weibull and Peppas functions in characterizing drug release profiles using an exact enumeraction scheme

S Casault and GW Slater.

Submitted to Int. J. Pharm

Testing the Weibull and Peppas functions in characterizing drug release profiles using an exact enumeration scheme

Sébastien Casault and Gary W. Slater*
Department of Physics, University of Ottawa, 150 Louis-Pasteur, Ottawa, Ontario K1N 6N5, Canada
(Dated: December 31, 2006)

Diffusion is often used as a primary method of transport in many drug delivery schemes. We present a systematic investigation of the Weibull and the Peppas functions as useful tools in quantifying mass transport in drug release related situations. The data is obtained from a 2D simulated hydrogel using an exact enumeration scheme. We note that there are distinct regimes for some of the free parameters which depend on obstacle density. Further, the free parameters in the fits are shown to be largely time-dependent and therefore cannot be used to infer fundamental characteristics of the underlying physical mechanism. We show that the Weibull function is more dependable in characterizing release profiles although one must be cautious when interpreting data due to the parameters' fluctuating nature.

Keywords: Diffusion; Weibull; Peppas; Hydrogels; Drug delivery; Exact-enumeration

I. INTRODUCTION

A controlled release mechanism is often critical to successfull drug therapy. Drug delivery usually consists of the timely release of a specific substance in order to be successful. Many drug release platforms rely on diffusion of a drug through a polymeric network such as a hydrogel in order to control the rate of release [1, 2]. Since the design of the hydrogel platform can be modified, the release profile can be tailored to meet the needs of the specific therapy being used [3, 4] (*e.g.*, constant release, pulsed released, etc.). For this reason, it is important to study the dependence of diffusion on the conditions that arise in such hydrogels (*e.g.*, hydrogel density, placement and degree of order of the obstacles). Proper characterization of release profiles (*i.e.*, drug release as a function of time) is thus crucial in determining if a specific drug release platform is appropriate.

There are various effective ways of characterizing the release profile of a solute escaping a hydrogel. Many of these approaches give empirical relationships with several free parameters which allow the description of release profiles under a variety of conditions. One of the most widely used methods comes from the field of materials science. For example, Weibull first introduced a stretched exponential to quantify fatigue data [5] and it was later adapted for pharmaceutics by Langenbucher [6] to describe the drug release as a function of time. It has been used many times to date and continues to be of great empirical importance [7–10].

Korsmeyer et al. [11] have proposed another fitting function which is often used to describe the release profile. This so-called Peppas function seems to be attracting mixed reactions [12]. Critisism is generally directed towards its inability to describe the release profile over the entire duration of drug release [13]. However, it is often used in experimental analysis and thus warrants careful examination [14, 15].

This article is a systematic study on fitting drug release profiles from fully loaded and non-degrading simulated hydrogels of varying densities and sizes. We use a two-dimensional (2D) exact lattice enumeration approach that will be discussed in further details in section III in order to obtain exact diffusional release profiles from our hydrogels. The density of the hydrogel is modeled by a certain concentration of unmovable obstacles. Also, fully loaded refers to the fact that each non-obstacle site contains an equal initial drug concentration and that release immediately begins at $t > 0$. We investigate the relationship between the Weibull and the Peppas functions and contrast the differences between the two fits by examining the dependence of the parameters on the enumeration time and gel structure using data obtained from our exact enumeration approach. We study the relationship between the free parameters in the fitting functions and the different possible geometries of a hydrogel and possible release kinetics in a controlled theoretical environment and using exact numerical results with no error bars which are usually associated with experimental data.

We begin with a brief overview of the Weibull and Peppas functions (and nomenclature) followed by an explanation of the enumeration method used to compute drug release profiles. Release profiles are analyzed using the Weibull and the Peppas fits for various hydrogel geometries (*i.e.*, a gel composed of periodic obstacles and one of randomly placed obstacles). We focus on the dependence of their associated free parameters with time. We illustrate that a marked change in behaviour of the Weibull function occurs as the hydrogel's density is increased towards the percolation threshold for obstacles placed randomly. We show that performing a fit on release profiles starting from varying initial times can also yield different values for the parameters in the Weibull fit. We conclude by investigating the effects of system size on release profiles.

*Electronic address: gary.slater@uOttawa.ca

II. THEORY

The Weibull [5] and the Peppas functions [11] are frequently used to describe the drug release process (*i.e.*, the total drug released from a hydrogel as a function of time for a specific structure). For a fully loaded hydrogel, the Weibull function is given by

$$\tilde{\Gamma}(t) = \frac{\Gamma(t)}{\Gamma(\infty)} = 1 - \exp\left[-\left(\frac{t}{t_\beta}\right)^\beta\right] \qquad (1)$$

where $\tilde{\Gamma}(t)$ represents the normalized cumulative amount of drug released at time t. The specific functional form of $\tilde{\Gamma}(t)$ is determined by the exponent, β, a characteristic time t_β and the asymptotic release amount $\Gamma(\infty)$ (the latter is equal to the total amount of drug present in the hydrogel at $t = 0$, Γ_0, if no drug particle is trapped inside the hydrogel). We can write $\Gamma(t)$ as:

$$\Gamma(t) = \Gamma_0 - \int_0^t \int_\Omega C(\vec{r}, t')\mathrm{d}\Omega\mathrm{d}t' \ . \qquad (2)$$

$C(\vec{r}, t')$ describes the drug concentration at position $\vec{r}$ at time t' and Ω represents the volume (or area in two-dimensions) of the hydrogel. Note that $\tilde{\Gamma}(t \to \infty)$ can be $< \Gamma_0$ if some drug particles remain trapped inside the hydrogel. The exponent β determines the shape of the $\tilde{\Gamma}(t)$ versus time curve. The curve can be exponential ($\beta = 1$), sigmoidal and S-shaped with initial upward curvature ($\beta > 1$), or parabolic with a higher initial slope ($0 < \beta < 1$) [7].

The Peppas fit is given by the following relationship:

$$\tilde{\Gamma}(t) = \frac{\Gamma(t)}{\Gamma_0} = \left(\frac{t}{t_\alpha}\right)^\alpha \qquad (3)$$

where the exponent α is related to the dynamic properties of the release profile. The choice of a normalization factor is arbitrary here. The initial load Γ_0 is a logical choice, and the resulting time scale t_α can then be compared to t_β for short times ($\tilde{\Gamma} \ll 1$). The Peppas equation cannot be used to model the escape at long times since it is not bounded as $t \to \infty$. For this reason, only the first part of the release curve is usually taken for this fit ($\tilde{\Gamma}(t) \lesssim 0.6$) when used experimentally. However, Rinaki *et al.* [15] have shown that the Peppas fit can be well suited to describe the release curve well beyond $\tilde{\Gamma}(t) \simeq 0.6$. In principle, $\alpha \to \beta$ as $t \to 0$ and so α and β may both depend on t. This is shown in the following sections using our exact enumeration model.

Both of these empirical fits lack information about the fundamental mechanism responsible for altering the diffusion as well as the physical properties of the hydrogel. Some authors have associated kinematic diffusion arguments to the value of the free parameters [9, 11, 13, 16] with varried success.

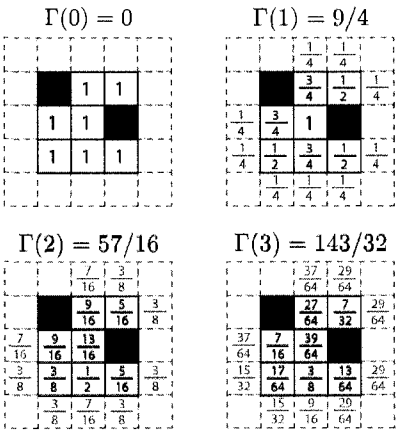

FIG. 1: Time evolution of a 3×3 system of particles undergoing diffusion on a 2D square matrix with two obstacles (black) ($\mathcal{C}_{\mathrm{obst}} = 2/9$). We use a fully loaded hydrogel and the initial configuration is shown at $t = 0$ ($C_{xy}(0) = 1$ on each non-obstacle site). The outer boundary is shown in grey and the cummulative release from the hydrogel, $\Gamma(t)$, is shown after each time step.

III. ENUMERATION METHODOLOGY

We use a lattice enumeration method based on the model proposed by Majid et al. [17] and used in a previous study by the authors in order to obtain exact numerical results for problems related to short time diffusion, escape rates and transient effects. We can alter diffusion properties by inserting obstacles which hinder the movement of the diffusing particles. We study here the effects of systematically increasing the obstacle concentration, $\mathcal{C}_{\mathrm{obst}}$, on a 2D square lattice towards the percolation threshold ($\mathcal{C}^*_{\mathrm{obst}} \simeq 0.408$ for a 2D square lattice with coordination number $z = 4$ [18]). We can also change the size of the hydrogel and note the associated effects on the release profile. Figure 1 illustrates the enumeration method by following solute diffusion through 3 consecutive time steps on a simple 3×3 2D square lattice with 2 obstacles ($\mathcal{C}_{\mathrm{obst}} = 2/9$). The boundary is shown in grey and the cumulative sum of drug that have escaped is shown at each time step, $\Gamma(t)$. We compute all possible particle trajectories of a solute based on its initial location and its probability to diffuse to any first nearest neighbour on the lattice.

In an isotropic 2D square lattice system, the probability to diffuse in any given Cartesian direction is $p_{\pm x} = p_{\pm y} = 1/4$. A given solute particle has an equal probability to diffuse (or jump) to any four of the neighbouring sites. Time is discrete and all particles must attempt a jump at each time step. A move is simply re-

jected (*i.e.*, the particle is reflected) if the neighbouring site is occupied by an obstacle.

The two-dimensional master equation which describes the probability of having a drug concentration $C_{xy}(t)$ on a free site at (x, y) at time t is:

$$\begin{aligned} C_{xy}(t+1) &= [C_{x-1,y}(t)(1-q_{x-1,y}) + C_{x,y}(t)q_{x+1,y}]\,p_{+x} \\ &+ [C_{x+1,y}(t)(1-q_{x+1,y}) + C_{x,y}(t)q_{x-1,y}]\,p_{-x} \\ &+ [C_{x,y-1}(t)(1-q_{x,y-1}) + C_{x,y}(t)q_{x,y+1}]\,p_{+y} \\ &+ [C_{x,y+1}(t)(1-q_{x,y+1}) + C_{x,y}(t)q_{x,y-1}]\,p_{-y}. \end{aligned} \tag{4}$$

In this equation, $q_{x,y}$ is the site occupation index; its value is 1 if the site at (x, y) is occupied by an obstacle and 0 if there is no obstacle. For a given system, the value of $q_{x,y}$ is fixed for all lattice sites and is determined by the structure of the hydrogel under investigation. As schematically illustrated in figure 1, the calculation is done iteratively, from an initial drug concentration $C_{xy}(0)$ for each site on the lattice. Solute particles do not interact with each other.

In order to model drug release from a finite-sized hydrogel system, one imposes absorbing boundary conditions $p_{\pm x} = p_{\pm y} = 0$ on the outer surface of the hydrogel structure. The cumulative amount of drug escaping through this boundary is the sum of all those probabilities which have crossed the boundary up to time t (also shown on figure 1).

It is also possible to implement a stochastic mechanism by which to simulate various active effects (*e.g.*, moving obstacles, degradation of the hydrogel, etc.). In principle, one could also apply surface kinetic effects (*e.g.*, *sticky* obstacles, resistance to escape at the boundary, pH or viscosity gradients at the surface of the hydrogel, etc). These effects will not be studied in this article.

If the various local concentrations $C_{xy}(t)$ (including those in the absorbing layer) are grouped into a column vector $|C(t)\rangle$ with s elements (one for each lattice site; note that we use Dirac's bracket notation), equation 4 can be rewritten as a matrix equation

$$|C(t+1)\rangle = \mathbf{T}|C(t)\rangle. \tag{5}$$

The $s \times s$ Markovian transfer matrix $\mathbf{T}$ (which depends entirely on the positions of the obstacles) provides a simple iterative method of transforming the distribution at time t into the one at time $t+1$, where t is an integer. Using this notation we can write the initial total amount of drugs present in the system in discretized form

$$\Gamma_0 = \sum_{xy} C_{xy}(0) \tag{6}$$

and it follows that the total released drug at time t is

$$\Gamma(t) = \Gamma_0 - \sum_{xy} C_{xy}(t)\ . \tag{7}$$

IV. RESULTS

A. Diffusion out of a circular disk with no obstacles

We begin by studying the relationship between α and β as a function of total simulation time. We simulate diffusion on a fully loaded circular disk (there are no obstacles) constructed inside a 200×200 square matrix (*i.e.*, radius $r_0 = 100$). We can write a diffusion time for the system, τ, as

$$\tau \simeq \frac{r_0^2}{4D} \sim \frac{10^4}{1} \sim 10^4 \tag{8}$$

where D is the diffusion coefficient and the product $4D$ is of order unity here. We thus expect our characteristic times t_β and t_α to be of order 10^4.

The drug release profile together with the associated fits can be seen in figure 2. The drug release was simulated up until $\tilde{\Gamma}(t) = 0.999$ in order to study a large portion of the profile. For the Weibull fit, $\beta_{0.999} = 0.718$, $t_{\beta,0.999} = 4192$ and for the Peppas fit, $\alpha_{0.999} = 0.216$, $t_{\alpha,0.999} = 30603$. Because there are no obstacles (trapped drugs), $\Gamma_0 = \Gamma(\infty)$. As expected, it is quite apparent from the figure that the Peppas fit should not be used to characterize the release profiles at long times. On the other hand, the Weibull function provides a good fit over the whole range of the release profile.

Figure 3 shows the behavior of $t_{\alpha,\beta}$, as a function of simulation time for both fitting functions. When using the Peppas fit, the value of t_α is highly dependent on the portion of the release profile used. After $t \simeq 5000$, the value of t_α diverges approximately linearly. The characteristic time, t_β in the Weibull function converges to $t_\beta = 4180 \pm 30$. All asymptotic values for t_β and later, $\beta_{t\to\infty}$ were obtained by fitting the long time portion of the graph with an exponential of the form: $y(t) = y_\infty + Ae^{-Bt}$ and by extracting y_∞.

Papadopoulou *et al.* have made an argument for the relationship between the two exponents [9]. They propose that the linear relationship they observed between α and β is indicative of a physical connection to the release mechanism. They also propose that the value of β is inversely proportional with the amount of disorder in the medium. These suggestions can easily be tested here.

Figure 4 shows the exponents α and β from equations 3 and 1, respectively, as a function of simulation time. The inset shows the same data on a semi-log plot. As $t \to 0$, we observe $\alpha \to \beta$. This is expected since a series expansion of equation 1 yields, to first order, equation 3. Similarly, the two time constants converge when $t \to 0$. However, α and β diverge quite fast and, suprisingly, the divergence starts well below the characteristic time obtained for the Weibull fit.

The value of α is not reliable and decreases approximately linearly with time for $t > 5000$. The profile of the exponent in the Weibull function has an intriguing feature which can be clearly seen in the inset of figure 4. The value of β starts at $\beta = 0.748$ and decreases to

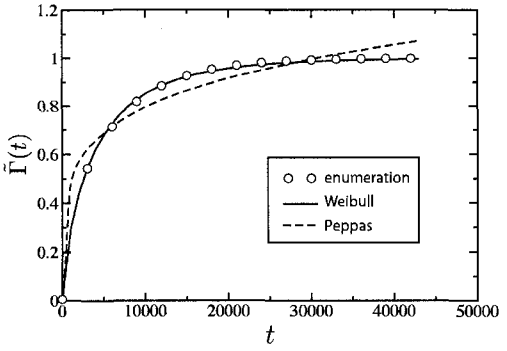

FIG. 2: Normalized cumulative release as a function of time for the case of no obstacles. The release was permitted to reach $\tilde{\Gamma}(t) = 0.99$ in order to observe long time release dynamics. The fitting parameters are: for Weibull $\beta_{0.99} = 0.718$, $t_{\beta,0.99} = 4192$ and for Peppas $\alpha_{0.99} = 0.216$, $t_{\alpha,0.99} = 30603$.

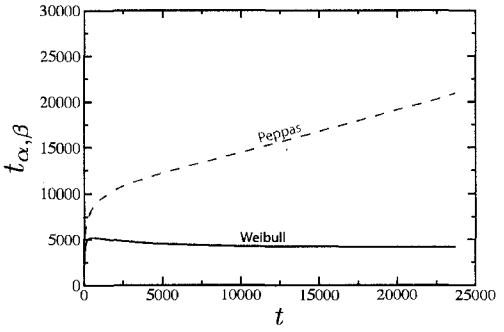

FIG. 3: Free parameter $t_{\alpha,\beta}$ as a function of the simulation time for the case of no obstacles. When using the Peppas function, t_α is dependent on simulation time and diverges nearly linearly above $t \simeq 5000$. However, when using the Weibull function, the characteristic time converges to $t_\beta = 4180 \pm 30$ after an initial peak value $t_\beta = 5191$ which occurs at simulation time $t = 592$.

reach a minimum value of $\beta = 0.563$ at $t = 592$ and then slowly converges to $\beta_{t\to\infty} = 0.728$.

Contrary to the proposed argument [9], there does not seem to be any physical significance to the diverging value of α with respect to β other than perhaps an indicator of the portion of the release profile used in the fit. Also, since both values (especially the parameters in the Peppas fit) are dependent on time, one must be careful when comparing fits from different release profiles. Different values of β cannot be indicative of the transport mechanism: indeed, we are definitely in the purely Fickian diffusion limit here (there is no hydrogel) and observe a wide range of β values. However, when using the Weibull

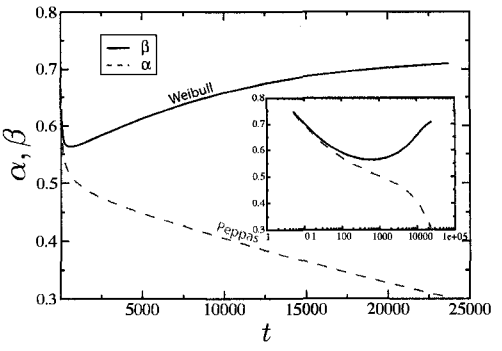

FIG. 4: Exponents used in the Peppas and Weibull functions with respect to simulation time for diffusion with no obstacles. As expected, $\alpha \to \beta$ for short times. The value of α is always dependent on the portion of the release profile used in the fit. It decreases approximately linearly with time after $t \simeq 5000$. The Weibull function's exponent converges to $\beta_{t\to\infty} = 0.728$ after reaching a minimum at $t = 592$. The inset shows another view of the same data on a semi-log plot. The minimum occurs at $\tilde{\Gamma}(592) = 0.25$ making it a non-negligeable portion of the release profile.

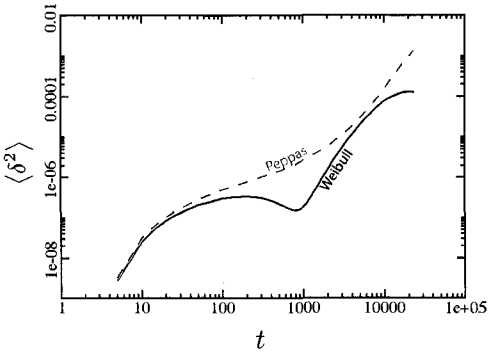

FIG. 5: Mean squared error on the fits as a function of the time used on a log-log plot for diffusion with no obstacles. Surprinsingly, both fits are fairly good over a large portion of the release profile. The two curves start diverging at $\Gamma(6000) = 0.6$ where the relative error is 0.01%. As expected, the error on the Weibull function is less than that of the Peppas fit and reaches a maximum value of $\langle \delta^2 \rangle = 1.3 \times 10^{-4}$. There is also an interesting region between $t \simeq 200$ and $t \simeq 1000$ where the error on the Weibull fit actually decreases.

function, the exponent β stabilizes at $t \simeq 5t_\beta$. This can be a good rule of thumb when characterizing a release profile with this function.

The mean error squared of the fits diverge as one tries to fit a larger portion of the release data when using the Peppas fit (see figure 5). Amazingly, the errors on the two

fits only start diverging significantly around $\tilde{\Gamma}(6000) \simeq 0.6$ – which is the usually reported highest limit for using the Peppas fit (this occurs at time $t \simeq t_\beta$). The two fits are surprisingly quite similar in terms of mean squared error until this point. However, the mean error reaches a maximum value of $\langle \delta^2 \rangle = 1.3 \times 10^{-4}$ when using the Weibull function. This error represents .01% of the value of $\tilde{\Gamma}(t) = 0.99$ at that point. There is an interesting feature in the curve for the Weibull function: the error is decreasing for a region between $200 < t < 1000$.

It is of interest to note that by fitting with the Weibull function at very short times, one can in fact obtain a decent estimate of the value of $\beta_{t\to\infty}$. Although the value of $\beta_{t\to\infty}$ can be estimated, t_β is not well estimated for short times and should be discarded. For this reason, one should fit at least up to $\tilde{\Gamma}(t) = 0.8$ or $t \simeq 5t_\beta$ of the release profile in order to obtain a dependable value for both β and t_β since these values seem to plateau in that region.

It is quite clear that the values of the free parameters in either fits cannot be interpreted to have any fundamental physical meaning since they are time-dependent. Further, when using the Weibull fit $0.563 < \beta < 0.748$ at different times during a single release profile. This variation cannot be attributed to non-Fickian diffusion or other geometrical properties since there are no obstacles present in the simulation.

B. Hydrogels composed of periodic obstacles

We now study the effects of increasing the density of obstacles in a hydrogel (*i.e.*, increasing $\mathcal{C}_{\rm obst}$) on the release profile. We begin by looking at the behaviour of the release profile in hydrogels with periodically placed obstacles in order to obtain exact results (see figure 6a). The system used here is a circular hydrogel constructed inside a 200×200 square matrix. The release was simulated until $\tilde{\Gamma}(t) = 0.99$ for each simulation. Again, there are no trapped drugs here and $\Gamma_0 = \Gamma(\infty)$ for these gels. The cumulative drug release profiles can be seen in figure 7. As expected, increasing the obstacle concentration effectively slows the diffusion (*i.e.*, decreases the effective diffusivity of the drug).

We see the same qualitative behaviour as previously shown with the characteristic times, $t_{\alpha,\beta}$, as a function of simulation time (see figure 8). In the Peppas fit, t_α diverges approximately linearly for long times. By fitting with an exponential decay, we obtain the converging values of t_β for the Weibull function (given in Table I). The values of t_β as a function of $\mathcal{C}_{\rm obst}$ are plotted in figure 9. This shows a strikingly linear relationship of the form:

$$t_\beta(\mathcal{C}_{\rm obst}) = t_\beta(0)\left(1 + \frac{\mathcal{C}_{\rm obst}}{\mathcal{C}}\right), \qquad (9)$$

where $t_\beta(0) = 4180$ and $\mathcal{C} = 0.54$. The error bars are smaller than the symbols.

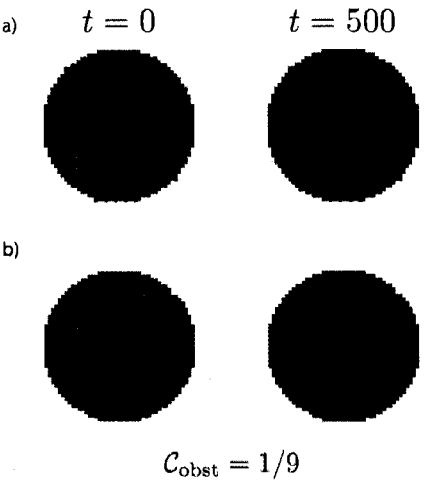

FIG. 6: Two circular 50×50 hydrogels with obstacles placed a) periodically and b) randomly. In both cases $\mathcal{C}_{\rm obst} = 1/9$ and the distribution of particles is shown at $t = 0$ and at $t = 500$. The concentration of drug particles ranges from high (red) to low (blue).

TABLE I: Asymptotic Weibull fitting parameters for a hydrogel composed of periodically placed obstacles.

$\mathcal{C}_{\rm obst}$	$t_\beta(t \to \infty)$	$\beta_{t\to\infty}$
0	4180 ± 30	0.728 ± 0.001
1/25	4460 ± 20	0.727 ± 0.001
1/16	4670 ± 20	0.727 ± 0.001
1/9	5080 ± 30	0.726 ± 0.001
1/4	6090 ± 30	0.725 ± 0.001

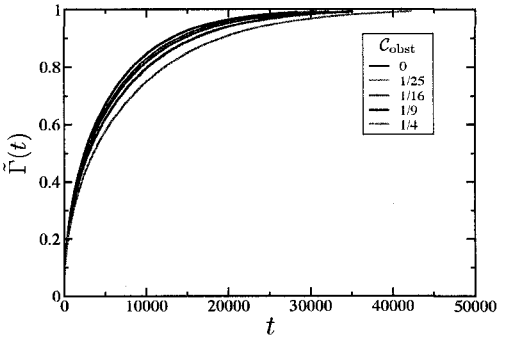

FIG. 7: Normalized cumulative drug release as a function of time for hydrogels of various periodic obstacle concentrations (shown in legend). The simulation was performed until $\tilde{\Gamma}(t) = 0.99$. Increasing the obstacle concentration effectively slows down the diffusion of drug.

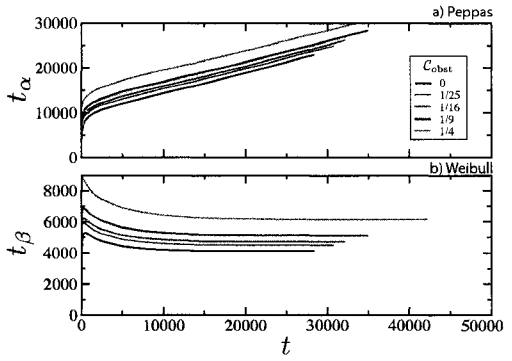

FIG. 8: Characteristic times, $t_{\alpha,\beta}$, as a function of simulation time in a) the Peppas fit and b) the Weibull function for hydrogels of various periodic obstacle concentrations (shown in legend). There is no significant qualitative change in behaviour of $t_{\alpha,\beta}$ as one increases the obstacle concentration other than a systematic increase of $t_{\alpha,\beta}$.

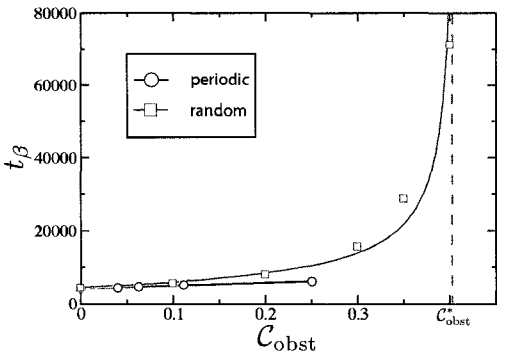

FIG. 9: Characteristic times, t_β, as a function of $\mathcal{C}_{\rm obst}$ for, ○ a system composed of periodically placed obstacles and, □ a system composed of randomly placed obstacles. There is a linear relationship between t_β and $\mathcal{C}_{\rm obst}$ for the periodic system whereas t_β blows up at $\mathcal{C}^*_{\rm obst}$ (dashed line) for the random system.

Figure 10 shows the exponents in the fits as a function of simulation time. Again, α is time-dependent and diverges from β as $t \to \infty$. The associated values of $\beta_{t\to\infty}$ are given in Table I. These results are consistent with each other and suggest that the asymptotic value of β does not depend on $\mathcal{C}_{\rm obst}$ in an ordered medium: $\beta_{t\to\infty} \simeq 0.727 \pm 0.001$.

The mean squared error of the fits increases smoothly for both fits (see figure 11). The error associated with both fits is low until $t \simeq t_\beta$, where the errors starts diverging for all obstacle concentrations. The error then reaches a maximum value for the case of the Weibull

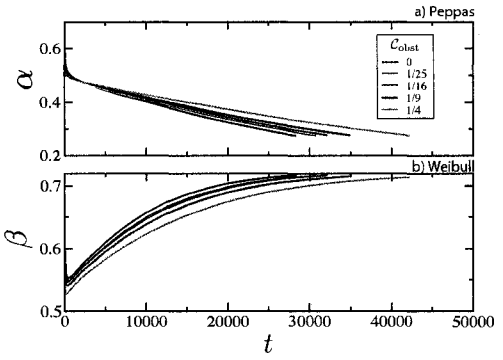

FIG. 10: Exponents used in the a) Peppas and b) Weibull functions with respect to simulation time for hydrogels of various periodic obstacle concentrations (shown in legend).

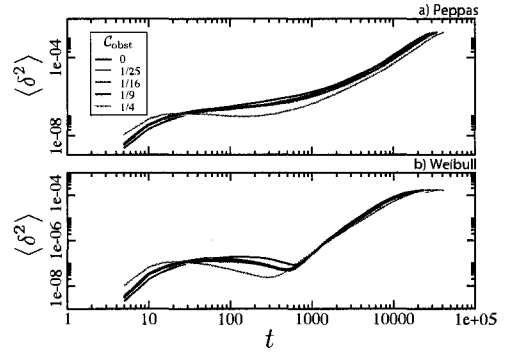

FIG. 11: Mean squared error on the fits as a function of simulation time shown on log-log plots for a) the Peppas fit and b) the Weibull function for hydrogels of various periodic obstacle concentrations (shown in legend). Again, both fits are fairly good over a large portion of the release profile. However, the error on the Peppas fit diverges while the error on the Weibull function reaches a maximum value.

function; each Weibull curve approximately has the same maximum value of $\langle\delta^2\rangle = 1.29 \times 10^{-4}$ (or $\simeq 0.01\%$ of $\tilde{\Gamma}(t)$).

For systems with periodically placed obstacles, we thus have an empirical expression for equation 1 which depends on $\mathcal{C}_{\rm obst}$:

$$\tilde{\Gamma}(t, \mathcal{C}_{\rm obst}) = 1 - \exp\left[-\left(\frac{t}{4180\left(1 + \frac{\mathcal{C}_{\rm obst}}{0.54}\right)}\right)^{0.727}\right] \quad (10)$$

where $\tilde{\Gamma} = \Gamma(t)/\Gamma_0$ since $\Gamma(\infty) = \Gamma_0$ here.

The fact that $\beta_{t\to\infty}$ does not seem depend on $\mathcal{C}_{\rm obst}$ in ordered media indicates that the mechanism of diffusion

remains unchanged in these highly ordered types of configurations. In fact, this indicates that we could obtain the same release profile by removing all the obstacles and including an equivalent viscosity in the hydrogel equal to

$$\eta(\mathcal{C}_{\text{obst}}) = \eta(0)\left(1 + \frac{\mathcal{C}_{\text{obst}}}{0.54}\right) \tag{11}$$

where $\eta(0)$ is the viscosity of the solvent phase in the absence of obstacles.

In conclusion, we note again that the value of β varies greatly depending on the simulation time for each release curve. Therefore, one must use caution when comparing release profiles fitted with the Weibull function.

C. Hydrogels composed of randomly placed obstacles

Complimentarily, we study the effects of randomly placed obstacles with various concentrations on the drug release profile. Again, we use a circular hydrogel constructed inside a 200 x 200 square lattice (see figure 6b). Note that the release was simulated until $\tilde{\Gamma}(t) = 0.90$ for each simulation. For each reported obstacle concentration, an average of $\tilde{\Gamma}(t)$ was performed over 500 realizations of disorder in order to obtain good statistical data due to the finite size of our hydrogel. The cumulative drug release profiles can be seen in figure 12. As expected, an increase in $\mathcal{C}_{\text{obst}}$ has a retarding effect on the drug release from the hydrogel. We show the release profile for $\mathcal{C}_{\text{obst}} = 0.40$ in this figure although the values of $t_{\alpha,\beta}$, α, and β will not be shown on the next figures due to the difference in orders of magnitude.

There is an increasing number of drugs which remain trapped inside the hydrogel as one increases the obstacle concentration. For this reason, one must perform the Weibull fits with $\Gamma(\infty) < \Gamma_0$ as a free parameter (from equation 1). There are two ways to obtain the amount of trapped drugs in our hydrogel: we can perform the fits with 3 parameters over a long portion of the release profile or we can actually calculate this value directly from our gels. In order to obtain a good estimate for this asymptotic value by fitting the function, one must allow the simulation time to be very large to get a good portion of the asymptotic part of the profile. The fitted values of $\Gamma(\infty)$ have been found to correspond to the calculated value of trapped drugs during test simulations. For this reason, we use the calculated values of the fraction of trapped drugs for $\Gamma(\infty)$ and use it to fit the normalized profiles $\tilde{\Gamma}(t) = \Gamma(t)/\Gamma(\infty)$ with the Weibull function. This reduces the number of fitting parameters to two (β, t_β).

Figure 13 shows $t_{\alpha,\beta}$ in the fits as a function of simulation time. The behaviour of the curves is similar to that observed in the previous sections. Again, the values of t_α for the Peppas fit diverge at long times whereas t_β converge to a unique value when using the Weibull function. There is a slight upward shift in the values of $t_{\alpha,\beta}$ obtained for low $\mathcal{C}_{\text{obst}}$ when compared to those obtained from a hydrogel composed of periodic obstacles. There is a sharp rise in the Weibull characteristic time for $\mathcal{C}_{\text{obst}} = 0.35$ and $\mathcal{C}_{\text{obst}} = 0.40$ (not shown). This is associated with the increasing tortuous nature of the hydrogel. The asymptotic values of t_β for these hydrogels can be seen in Table II. We can plot the value of t_β as a function of $\mathcal{C}_{\text{obst}}$ (see figure 9) and observe the characteristic time blowing up as it approaches $\mathcal{C}^*_{\text{obst}}$. These values were fitted with the empirical function:

$$t_\beta(\mathcal{C}_{\text{obst}}) = t_\beta(0)\left(1 + \frac{A\mathcal{C}_{\text{obst}}}{(\mathcal{C}^*_{\text{obst}} - \mathcal{C}_{\text{obst}})^\gamma}\right) \tag{12}$$

where the constants were found to be $A = 1.5 \pm 0.2$ and $\gamma = 0.7 \pm 0.1$ while the following were fixed $\mathcal{C}^*_{\text{obst}} = 0.408$ and $t_\beta(0) = 4180$. A series expansion of equation 12 yields values that are consistent with those obtained from equation 9 for $t \to 0$.

TABLE II: Asymptotic fitting parameters used in the Weibull function for a hydrogel composed of randomly placed obstacles. Note that the value of $\Gamma(\infty)$ was calculated during the enumeration. These values are for a system of size 200 x 200.

$\mathcal{C}_{\text{obst}}$	$t_\beta(t \to \infty)$	$\beta_{t\to\infty}$	$\Gamma(\infty)/\Gamma_0$
0.00	4180 ± 30	0.728 ± 0.001	1.00
0.10	5320 ± 50	0.728 ± 0.001	1.00
0.20	7700 ± 80	0.717 ± 0.001	1.00
0.30	15500 ± 300	0.629 ± 0.001	0.98
0.35	28600 ± 500	0.590 ± 0.001	0.97
0.40	71000 ± 1000	n/a	0.89

Figure 14 shows the value of the fitting exponents as a function of time. As observed earlier, α decreases for long times and cannot yield any significant result. Interestingly, all the curves cross at $t \simeq 7000$. Also, the values obtained for $\beta_{t\to\infty}$ are now distinct for each obstacle concentration for these system sizes (*i.e.*, $\beta = \beta(r_0)$). These values are shown in Table II for increasing $\mathcal{C}_{\text{obst}}$. We could not obtain a reliable value for $\beta_{t\to\infty}$ for the case of $\mathcal{C}_{\text{obst}} = 0.40$.

Finally, we can study the mean square error on the fits as a function of simulation time (see figure 15). The qualitative behaviour of the error does not seem to be very different from that observed previously.

In periodic systems, the diffusing drugs have a clear path out of the system and have no risk of encountering dead-ends or long tortuous obstacle clusters that are common in random systems.

D. Size-dependence of β in the Weibull fit

Let us now examine the effects of the obstacle concentration, $\mathcal{C}_{\text{obst}}$, and system size, L, on the β parameter in the Weibull function. Every system in this section

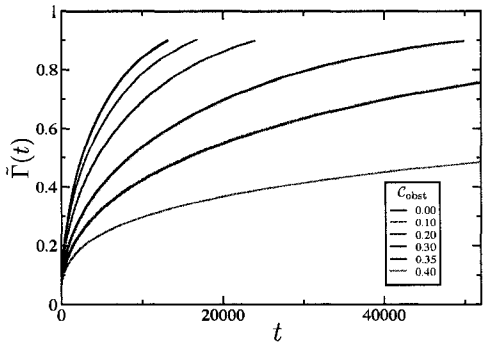

FIG. 12: Normalized cumulative release as a function of time for randomly placed obstacles of increasing concentration, C_{obst} (shown in legend).

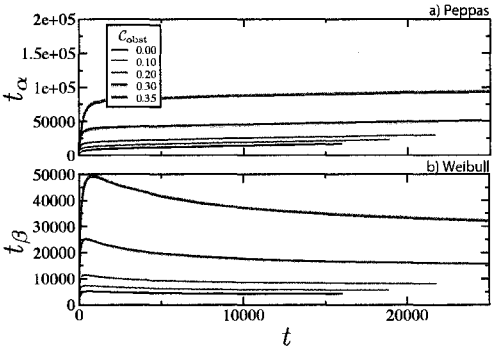

FIG. 13: Characteristic times $t_{\alpha,\beta}$ as a function of simulation time for a) the Peppas fit and b) the Weibull function for randomly placed obstacles. There is a large systematic increase of the characteristic time for the case of $C_{obst} = 0.35$ and of $C_{obst} = 0.40$ (not shown) although the curves behave in similar fashions.

is constructed with randomly-placed obstacles following the same method as explained in section IV C except with varying radii depending on the studied system size. The average values of $\beta_{0.9}$ are shown together with the associated standard deviation for 500 realizations of disorder.

The exponent $\beta_{0.9}$ as a function of inverse system size is shown in figure 16 for various values of C_{obst}. $\beta_{0.9}$ is obtained for every system by fitting up to $\tilde{\Gamma}(t) = 0.9$. This explains the slightly lower values of $\beta_{0.9}$ shown here as opposed to the previously reported values of $\beta_{t\to\infty}$. There is a tendency for $\beta_{0.9}$ to decrease as the system size increases for low values of C_{obst}. However, the trend is reversed for higher C_{obst}. The results indicate that as the system size is increased, $\beta_{0.9} \simeq 2/3$ independent of C_{obst}.

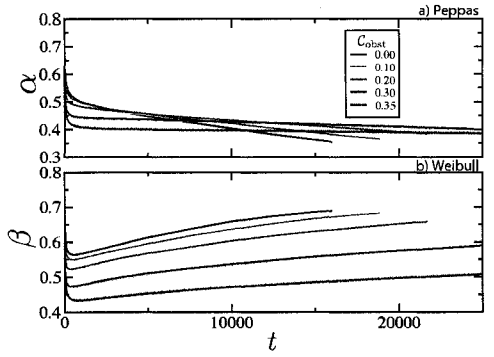

FIG. 14: Exponents a) α and b) β as a function of simulation time for randomly placed obstacles.

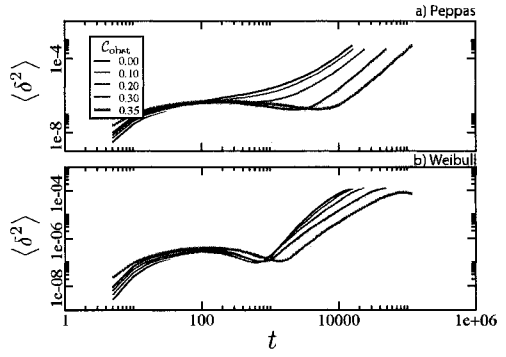

FIG. 15: Mean error squared as a function of simulated time for a) the Peppas fit and b) the Weibull function for randomly placed obstacles.

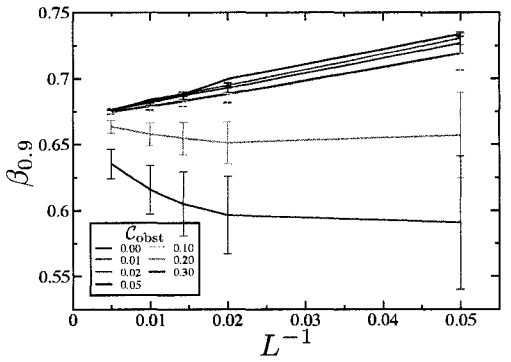

FIG. 16: Exponent $\beta_{0.9}$ as a function of inverse system size, L^{-1} for different obstacle concentrations, C_{obst}. The error bars represent the standard deviation observed over the 500 systems.

Diffusion in random systems typically follows three different time regimes. First, over a very short time scale, a particle diffuses as if it were in an environment free of obstacles or constraints (for our systems, this would last for a time of order unity and is thus irrelevant). The diffusing particle then explores the local structure of the environment, which slows it down substantially. During that period of time, it does not possess a unique diffusion coefficient since it has yet to discover the *typical* nature of the random system of obstacles. The randomness of the environment can in fact be characterized by a correlation length $\lambda(\mathcal{C}_{\rm obst})$. Until the particle has diffused over this length scale, its diffusion is anomalous and is strongly influenced by the details of the random distribution of obstacles. Finally, after it has diffused over distances larger than λ, the particle sees the average characteristics of the environment and its diffusion becomes normal (or Fickian) [17, 19]. The cross-over (or correlation) length increases with $\mathcal{C}_{\rm obst}$ and diverges at $\mathcal{C}_{\rm obst} = \mathcal{C}^*_{\rm obst}$. For finite-size systems such as those studied here, the overall drug release pattern will thus depend on the relative values of the system size L and the correlation length $\lambda(\mathcal{C}_{\rm obst})$. Whenever $L \gg \lambda(\mathcal{C}_{\rm obst})$, anomalous diffusion will have a negligible influence and the particle should see an average obstacle concentration and experience normal diffusion with a reduced diffusion coefficient $D(\mathcal{C}_{\rm obst}) < D(0)$. Just like in the case of periodically distributed obstacles, we then expect a universal Weibull exponent β. However, if L is comparable to (or smaller than) the correlation length $\lambda(\mathcal{C}_{\rm obst})$, anomalous diffusion will be dominating and the exact nature of the local random structure and the precise value of the ratio $L/\lambda(\mathcal{C}_{\rm obst})$ will play major roles. This is why the exponent $\beta_{0.9}$ is changing with system size L in figure 16; we also note the much larger error bars for higher concentrations, indicating the increased importance of anomalous diffusion. As L increases, anomalous diffusion plays a lesser role and all Weibull exponents converge towards the same value, as expected. In these larger systems, the increased obstacle concentration acts again as an effective viscosity which slows down the diffusive action of the drugs without affecting the shape of the release curve (*i.e.*, changing β). The asymptotic (*i.e.*, for an infinite system) value of $\beta_{0.9} \simeq 2/3$ is due to our choice of simulation parameters such as the upper fitting limit; an extrapolated value of $\beta_{1.0}$ should give a value consistent with that found for periodic systems or random systems with low obstacle concentrations (about 0.728, see Tables I and II).

E. Sliding window analysis of the release profile

Due to the nature of experimental setups, it is usually impossible to start release measurements from $\tilde{\Gamma}(t = 0) = 0$. There is usually a time lag before release measurements can take place that we denote as t'. Using the Weibull function and its three parameters (*i.e.*, $\Gamma(\infty)$, t_β, and β), we investigate the effects on β of fitting drug release profiles from an initial time $t' \geq 0$ up to the time where $\tilde{\Gamma}(t = 43707) = 0.999$. This is shown in figure 17 where β is plotted as a function of the lower time bound of the fit, t'. The asymptotic value obtained in section IV A of $t_\beta = 4180$ for $t' = 0$ is shown on the graph for comparison. The release profiles used here come from 2D circular disks constructed inside 200×200 square lattices with no obstacles (*i.e.*, the pure diffusion limit).

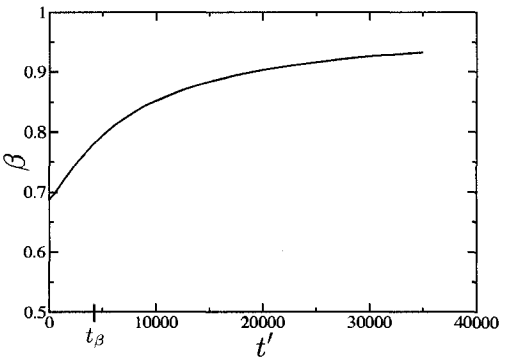

FIG. 17: Sliding window analysis of β as a function of a lower time bound t'. We show the results of the Weibull fit in the time interval between t' and the time where $\tilde{\Gamma}(t) = 0.999$. As expected, $\beta \to 1$ as the value of t' is increased. The asymptotic value of $t_\beta = 4180$ is shown for comparison.

We observe a value of $\beta(t' = 0)$ that is different (lower) from the one obtained in section IV A. This is due to the fact that we now chose to fit with $\Gamma(\infty)$ as a free parameter. As we increase the lower time bound of the fit, we obtain $\beta \to 1$ and recover the solution $\tilde{\Gamma}(t \to \infty) \sim e^{-t}$, as expected. There is also an inflection point in the curve at $t' \ll t_\beta$. The value of β obtained is very sensitive to the lower time bound suggesting that ignoring even a small portion of the initial drug release profile can have large effects on the associated Weibull function's fitting parameters. This is another example showing the lack of dependability when strictly using the Weibull function's parameters in order to categorize or compare drug release profiles.

V. CONCLUSION

We have provided a systematic investigation showing the behaviour of two widely-used empirical fits while representing drug release profiles from various hydrogels (and the free diffusion case). Our drug release profiles were obtained using an exact enumeration technique designed to model diffusion without the error bars that are usually associated with stochastic numerical and experimental techniques. We have shown that one must be careful when comparing fits from different release pro-

files since the free parameters were shown to be time-dependent. However, there is a stable regime for the free parameters when using the Weibull function which occurs around $t = 5t_\beta$. Verifying if whether or not one is using the Weibull function in its stable regime can be done iteratively in a laboratory setting by obtaining release data and fitting the Weibull function until the obtained value of t_β does not change significantly (stable regime). One should then only use the Weibull function to fit a release profile that contains data up to a time of at least $5t_\beta$.

We have also studied the effects of system size on the use of the Weibull function and have noticed finite size effects. We have shown that $\beta_{0.9}$ depends on the system size, L, for smaller systems and especially when approaching the critical obstacle concentration, $C_{\text{obst}} \to C^*_{\text{obst}}$. However, $\beta_{0.9}$ converges towards a constant value as the system size is increased regardless of C_{obst}. In large systems, the correlation length of the random distribution of obstacles is small compared to the size of the system and the effects of anomalous diffusion are negligible. The obstacle concentration acts like an effective viscosity retarding the diffusive motion of the drug molecules. This does not significantly alter the shape of the release curve.

Finally, we have shown that the portion of the release profile used to fit the Weibull function can have large effects on the associated release exponent, β. Essentially, β is not a reliable indicator of the release mechanism since we find a wide range of possible values of the fitting parameters – even in the free diffusion case when $C_{\text{obst}} = 0$.

Acknowledgments

The authors would like to thank M. Bertrand, M. Kenward, and E. C. J. Oliver for useful discussions. Computational analysis was supported by the High Performance Computing Virtual Laboratory (HPCVL). This work was financially supported by the Advanced Foods and Materials Network (AFMNet) and by the Natural Sciences and Engineering Research Council of Canada (NSERC) to GWS.

[1] E. Losi, R. Bettini, P. Santi, F. Sonvico, G. Colombo, K. Lofthus, P. Colombo, and N. Peppas, J. Contr. Rel. **111**, 212 (2006).
[2] W. M. Saltzman and W. L. Olbricht, Nature Reviews **1**, 177 (2002).
[3] D. S. Cohen and T. Erneux, J. Appl. Math. **58**, 1193 (1998).
[4] X. Liu, K. Nakamura, and A. M. Lowman, Soft Mat. **1**, 393 (2003).
[5] W. Weibull, J. Appl. Mech. **18**, 293 (1951).
[6] F. Langenbucher, J. Pharm. Pharmacol. **24**, 979 (1972).
[7] P. Costa and J. M. S. Lobo, Eur. J. Pharm. Sci. **13**, 123 (2001).
[8] K. Kosmidis, P. Argyrakis, and P. Macheras, Pharm. Res. **20**, 988 (2003).
[9] V. Papadopoulou, K. Kosmidis, M. Vlachou, and P. Macheras, Int. J. Pharm. **309**, 44 (2005).
[10] T. Schreiner, U. F. Schaffer, and H. Loth, J. Pharm. Sci. **94**, 120 (2004).
[11] R. K. Korsmeyer, R. Gurny, E. Doelker, P. Buri, and N. A. Peppas, Int. J. Pharm. **15**, 25 (1983).
[12] N. A. Peppas, Pharm. Acta Helv. **60**, 110 (1985).
[13] P. Lánský and M. Weiss, J. Pharm. Sci. **92**, 1632 (2003).
[14] K. Kosmidis, E. Rinaki, P. Argyrakis, and P. Macheras, Int. J. Pharm. **254**, 183 (2003).
[15] E. Rinaki, G. Valsami, and P. Macheras, Int. J. Pharm. **255**, 199 (2003).
[16] A. Dokoumetzidis, K. Kosmidis, P. Argyrakis, and P. Macheras, Basic Clin. Pharm. Tox. **96**, 200 (2004).
[17] I. Majid, D. Ben-Avraham, S. Havlin, and H. E. Stanley, Phys. Rev. B **30**, 1626 (1984).
[18] P. J. Reynolds, H. E. Stanley, and W. Klein, Phys. Rev. B **21**, 1223 (1980).
[19] M. J. Saxton, Biophys. J. **66**, 394 (1994).

4

Optimization of the initial drug concentration distribution

The generation of random numbers is too important to be left to chance.
(Robert R. Coveyou, 1915–1996)

4.1 Introduction

It was thought that we could perform an additional level of optimization in the early phases of this project. Namely, that we could not only optimize the placement of obstacles inside the hydrogel, but that we could also optimize the initial concentration distribution of drug, $C(\vec{r}, 0)$, such that it would not be homogeneous initially. This would potentially improve the quality of our drug release profile in terms of controlling the release characteristics. We used a Metropolis simulated annealing algorithm in order to find the optimal initial drug distribution profile for hydrogel structures previously optimized by the genetic algorithm. This hybrid optimization process unfortunately increases the execution time by more than a few orders of magnitude and was thus found to be inefficient for the purposes of our studies. Furthermore, it was not clear how such optimized distributions $C(\vec{r}, 0)$ could be prepared experimentally. Nevertheless, it has yielded interesting results and will briefly be discussed here.

Since our enumeration is a Markovian process and we have a simple iterative algorithm, it is relatively straightforward to alter the initial drug concentration for one site and immediately know its effect on the associated release profile for a hydrogel with a given obstacle distribution, as the following matrix equation demonstrates:

$$M(t) = \sum_{i=0}^{s} \mathbf{S}(t,i) C_0(i) \tag{4.1}$$

where $C_0(i)$ represents the concentration of drug initially on site i. $\mathbf{S}(t,i)$ is an $s \times s$ matrix which represents the probability of escaping at time t by a particle with initial location i, where s is the number of non-obstacle sites (*i.e.*, valid initial drug locations). Changing a drug concentration at site i simply alters the i^{th} value of vector $C_0(i)$ and the associated release profile can be determined relatively quickly by recalculating the product for one row only. As we will see in the next section, this lends itself quite well to the Metropolis algorithm where changing the drug concentration at site i can represent a trial microstate, ω_i. The quantity we wish to minimize is chosen as the absolute difference between our obtained release profile and an ideal one. It can be written as the "energy" of the system,

$$U = |M_{\text{ideal}}(t) - M(t)|, \tag{4.2}$$

where $M_{\text{ideal}}(t)$ is an arbitrary release profile we wish to obtain (*e.g.*, a constant drug release over a given period of time).

4.2 Metropolis simulated annealing

The Metropolis simulated annealing algorithm is a probabilistic Monte Carlo global optimum finder. The Monte Carlo technique were first proposed in 1949 by Nicholas Metropolis and Stanislaw Ulam as a statistical approach to studying differential equations [63]. Monte Carlo here refers to the use of pseudo-random numbers in order to generate various microstates during calculation. Minimizing correlation in the generated number sequence is a critical gauge of the quality of any computer-based number generator. An efficient number generator must also be relatively quick since random numbers are often needed in many iterations. For this reason, the Mersenne Twister algorithm was chosen for its overall efficiency and quality [64]. Incidentally, the name Monte Carlo was chosen in honor of Ulam's uncle who was a gambler.

The simulated annealing technique was devised in order to calculate the ground state of thermodynamic systems. Starting from a highly energetic (high temperature, T) state, the system is gradually crystalized to a state of minimal energy (low T). Following the same logic, it is thus possible to crystalize (minimize) any given physical property (*e.g.*, fitness parameter) of a well-defined system by slowly decreasing its pseudo-temperature. Consider a thermodynamic system with an average physical property $\langle\psi\rangle$ associated with some state ω in a large phase space Ω

$$\langle\psi\rangle = \int_{\Omega} \psi(\omega)\rho(\omega)\mathrm{d}\omega \tag{4.3}$$

and where $\rho(\omega)$ is the associated probability density. The system is at equilibrium at a certain temperature T and with total energy $U(\omega)$ for a given microstate. We can write Eq 4.3 approximately in discrete conformational space as an average of n *randomly* generated states ω_i using the appropriate thermodynamic probability density $\rho = \exp\left(-U(\omega)/k_B T\right)$:

$$\langle\psi\rangle \simeq \frac{1}{n}\sum_{i=1}^{n} \psi(\omega_i)\mathrm{e}^{-U(\omega_i)/k_\mathrm{B}T}. \tag{4.4}$$

Importance sampling is then used to generate states, ω_i^*, which are distributed according to the probability density function. The average value of ψ then becomes

$$\langle\psi\rangle \simeq \frac{1}{n}\sum_{i=1}^{n} \psi(\omega_i^*) \tag{4.5}$$

and can effectively be computed numerically.

Later, in 1953, Metropolis *et al.* proposed a method for generating these *ideal* states, ω_i^*, in a computationally convenient fashion [65]. The algorithm can be summed up as follows:

1) Establish an initial microstate (drug concentration distribution), ω_0;
2) generate a random trial change in the microstate (change the concentration at one site), ω_1;
3) compute $\Delta U = U(\omega_1) - U(\omega_0)$;
4) if $\Delta U \leq 0$, accept ω_1;
5) else if $\Delta U > 0$, accept ω_1 with probability $\mathrm{e}^{-\Delta U/k_\mathrm{B}T}$;
6) else, retain ω_0 as the state.

One then repeats this process a large number of times for each value of T. Thus the idea of simulated annealing is that one should systematically lower the value of T in order to *freeze* the

FIGURE 4.1 Optimized hydrogel of radius $r_0 = 31$. The obstacles are in black and the initial drug concentration is shown ranging from low (blue) to high (red). The outer boundary of the hydrogel is schematically shown as the grey dashed line. Notice all the familiar structures found in the previous optimizations. Namely, the creation of an obstacle boundary somewhere in the hydrogel and a high concentration of drug near the centre to help curtail any strong initial drug peak.

system in its phase space optimum (*i.e.*, ground state). This yields progressively better solutions (*i.e.*, drug release profile which increasingly resemble $M_{\text{ideal}}(t)$). The following section presents a typical hydrogel obtained making use of this optimization scheme.

4.3 Results

We present results obtained using our novel hybrid optimization technique. The optimization algorithm resembles the one presented earlier using the genetic algorithm except that at each generation, the simulated annealing optimization finds an optimal initial drug distribution for every hydrogel and then assigns the fitness parameter based on the release profile obtained from this optimized obstacle *and* initial drug distribution. The hydrogels with the obstacle and drug distributions which best favour a controlled rate of drug release from each such generation are kept to form the next generation and the algorithm repeats this process for a given number of genetic generations. The algorithm can be described as follows:

1) Initialize a starting hydrogel population by randomly placing obstacles;

2) Perform simulated annealing to find the optimal load distribution $C(\vec{r}, \theta, 0)$ for each hydrogel and obtain the resulting fitness parameter;

3) Rank hydrogels according to their fitness parameter;

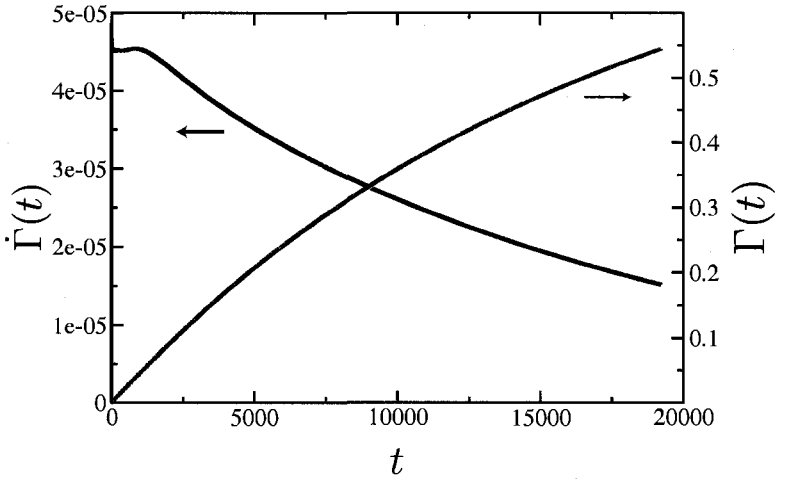

FIGURE 4.2 Shown are the rate of release (black) and the total release (red) as a function of time for the optimized hydrogel. The rate of release is constant until it gradually starts decreasing around $t \simeq 2500$.

4) Keep a certain number of these *fit* parents for creation of next generation;

5) If not last generation, empty drug from hydrogels and perform genetic swaps with parents. Form next generation of hydrogels, return to step 2;

6) Else, an optimal hydrogel structure has been found.

We used a small hydrogel of radius $r_0 = 31$ (see Figure 4.1) since the annealing optimization is computationally intensive. The associated obstacle and drug concentration distributions found as a result of using both optimizations is shown at $t = 0$; most of the drug is located near the centre of the hydrogel where it is enclosed by an obstacle barrier (black) created by the genetic algorithm. This optimized structure is the result of 17 genetic generations where each generation is composed of 100 specimens. The genetic operation used here randomly swaps 2 rings of thickness equal to $r_0/2$ lattice sites between 2 *fit* parents from the previous generation (*i.e.*, two chromosome swap in the genetic algorithm). The mutation rate is set at 3%. The fitness parameter is chosen as a horizontal line of height equal to

$$M_{\text{ideal}} = \left[\int_\Omega C(\vec{r}, \theta, 0) \mathrm{d}\Omega\right]^{-1} . \tag{4.6}$$

Each time a specimen is created (using these two genetic operations), its initial drug concentration distribution was optimized using the Metropolis algorithm with the following parameters: the number of Monte Carlo iterations (as defined in Eq 4.5), $n = 150,000$ per temperature step, the value of $k_{\mathrm{B}}T$ was lowered from 10^{13} down to 0 in 2.5×10^{11} increments. The number of Monte Carlo steps, n, is chosen to be sufficiently large in order to (hopefully) study the entire solution "phase space". In order to obtain good statistical data, the trial microstates ω_i^* (*i.e.*, changes to the drug concentration distribution) are chosen to maintain their acceptance rate at a value near 0.5 or lower for each temperature step [33, 66]. There is somewhat of a circular logic deficiency in this algorithm whereby altering the drug concentration distribution alters the release profile and so does altering the initial obstacle positions. Ideally, both of these parameters should be altered simultaneously although this would require more computing power. This hybrid technique was seen as a good compromise for optimizing both parameters.

Recall page 37 where the case of the fully loaded hydrogel is investigated. The created obstacle boundary seen here is strikingly similar to the one created for the fully-loaded hydrogel except that the simulated annealing was now able to attenuate the effects of a strong initial drug release peak by removing drugs from near the outer boundary. This seems to be a favourable structure in order to obtain a constant drug release over long times. The release rate (black) as well as the total release (red) as a function of time indicate that the drug release has been optimized to a certain extent (see **Figure 4.2**). As seen, the release rate is quite constant $\dot{M} \simeq 4.5 \times 10^{-5}$ up until $t \simeq 2500$ or $M(t) \simeq 0.1$. After which, the rate gradually decreases until the enumeration ends when $M(t) = 0.55$.

An efficiently controlled rate of release could thus be obtained for longer times; however, as mentioned before, this algorithm is quite demanding in terms of computing power and so only a limited number of genetic generations can be performed while maintaining a limited number of specimens per generation. Also, the annealing algorithm was only finding a constant rate of release over a small portion of the drug release profile (up until $M(t) \simeq 0.1$). The size of the hydrogel is also quite limited in this test example. Nevertheless, this novel technique will be of interest as computing power increases with (seemingly) no limit! A more efficient alternative at this point is the scheme proposed in Chapter 2 where a single optimization algorithm is used to find the number and placement of drug reservoirs, all of equal initial drug distribution. This scheme produced highly controlled drug release profiles without the simulated annealing algorithm.

5

Conclusion

People do not like to think. If one thinks, one must reach conclusions. Conclusions are not always pleasant.
(Helen Keller, 1880–1968)

The work presented in this thesis contributes to our knowledge of drug release from polymeric hydrogels, and specifically: the effects of geometry and design of the hydrogel, and how to reliably characterize release profiles. In the literature, drug release profiles are usually described using one of various empirical functions with varying success. Some have sought to establish a direct link between the free parameters in these functions and their associated diffusional mechanism. We have presented a systematic study of these free parameters under theoretically controlled conditions and have found no conclusive links. We have also presented an effective scheme that one may use in order to tailor the geometry of a hydrogel to obtain a functional form of the drug release profile using a combinatorial technique. This was performed using a genetic optimization algorithm that was designed and implemented specifically for this research. All drug release profiles were obtained using the exact enumeration scheme presented earlier. This numerical technique provided drug release profiles devoid of error bars (that are usually associated with experimental and/or numerical results).

There are many fortunate advantages to using the exact enumeration scheme in order to obtain diffusional drug release profiles from simulated hydrogels. For one, the algorithm lends itself very well to operational speedup techniques on current computing devices (*i.e.*, efficient cache

utilization, intelligent array scanning, etc.) due to its iterative nature. This allowed us to perform a relatively large number of enumerations and obtain an impressive collection of data which effectively helped guide our research. The enumeration data has also allowed us to obtain exact drug release profiles from a wide variety of hydrogel structures. As we have shown, these non-equilibirum (short time) data usually tend to be noisy when using conventional Monte Carlo diffusion simulations – especially in the high obstacle concentration limit where we may venture into the realm of anomalous diffusion. Thus, the main advantage of using the exact enumeration is that we are able to obtain the entire drug release profile in all its details without fear of missing important information or having error bars (or noise) which may obscure interpretation. Using this scheme, we have conclusively shown (see Chapter 3) that two widely used empirical functions, for example, do not fit the profile perfectly and that their free parameters actually vary depending on the portion of the release profile used in the fit and therefore must be used with caution.

The empirical characterization functions studied were the Peppas and the Weibull functions. The latter was shown to be better suited in representing a drug release profile coming from a large number of varying hydrogel structures. The Weibull function fits drug release profiles relatively well independently of the obstacle concentration which explains its importance in the literature. It is also possible, as we have shown, to solve the diffusion equation analytically for certain initial conditions and compare it to our exact drug release results. The drug release profiles coming from our enumeration are shown to be in excellent agreement with the analytical theory for the case of low obstacle concentration. However, as one increases the obstacle concentration, the diffusion coefficient becomes dependent on the position and we can no longer obtain an analytical solution (nor the functional form of the coefficient for that matter).

The drug release profile is shown to change its behaviour as the obstacle concentration is increased (*e.g.*, the profile flattens). For this reason, many have tried to equate a change in the fitting parameters of the Weibull profile with this change in diffusional behaviour. The free parameters obtained by fitting a given release profile with the Weibull function would then be indicative of the release mechanism. If true, this would offer a powerful tool in analyzing transient diffusion problems and the associated physical mechanism involved. Although the Weibull function is good at fitting drug release profiles, its associated free parameters are not consistent and actually depend on many factors (*e.g.*, the portion of the profile used in the fit, the time used to start the fit, etc.). One must thus use extreme caution when comparing various drug release profiles coming from different hydrogels solely using the Weibull function. We have presented certain guidelines to

interpret and compare drug release profiles using this function with more reliability since there are regimes where the free parameters tend to converge to fixed values. Therefore, we have concluded that one should fit the Weibull function up to $t \geq 5t_\beta$ as a good rule of thumb. This can be done experimentally by iteratively fitting a larger and larger portion of the drug release profile until one notices the value of t_β stabilizing.

We have carried out enumerations on simulated hydrogels of given sizes and have found potential finite size effects in our drug release profiles. We have briefly shown that the Weibull function's free parameters depend on system size and the effect becomes more important as one increases the obstacle concentration, as expected. Surprisingly, we have shown that the exponent in the fit seems to tend to a single value independently of the obstacle concentration as the size of the system is increased. It is probable that the fitting parameter does not actually depend on the obstacle concentration for infinite systems since the onset of anomalous diffusion only occurs close to the percolation threshold in such hydrogels. This would also mean that the analytic solution is a good description of the drug release process as long as $r_0 \gg R_{CR}$. Studying the positional dependence of the coefficient of diffusion as one increases the obstacle concentration toward the percolation threshold would be interesting. This could lead to a theory on finding the functional form of the coefficient of diffusion in complex structures.

It is possible to use a genetic optimization algorithm in order to control the functional form of the drug release profile and drastically alter it such that none of the traditionally used empirical functions could be used to properly its characteristics. Using the same exact enumeration approach to find the release from simulated hydrogels, we were able to alter the location of obstacles within the release platform opportunistically in order to obtain release profiles that were constant over long times. With the help of the optimization algorithm, we were able to notice specific structural qualities of our optimal hydrogel. For example, we have consistently observed the creation of an obstacle boundary near the edge of the release platform and concluded that it must play a critical role in obtaining our desire rate of release. Also, the obstacle concentrations tended to be very close to the percolation threshold in at least one region (usually located near the outer boundary) of each of our optimal hydrogel structures indicating that a constant rate of release was favoured in fractal structures from which anomalous diffusion arises. We have studied various hydrogel geometries under this scheme (*e.g.*, round capsule, transdermal-type device) and also the impact of varying the initial location of the drug particles.

The amount of control we had over the release profile was measured with a fitting parameter (a mathematical criterion which ranked the level of "niceness" of a certain profile with respect to an ideal one) before an adequate one was found. It is by changing this fitness parameter that one may later choose to experiment in obtaining other various forms of release profiles (*e.g.*, pulsed release, slowly increasing release, etc.). Also, it would be quite interesting to model various real-life properties of a hydrogel. Some of these effects could be straight forward to implement in our existing model such as hydrogel-drug affinity/repulsion. This could be done by altering the probability of diffusing to a nearest neighbour depending on the location of obstacles. We could introduce some bias in the diffusion in a similar fashion which could represent a pH gradient or external electric field (if the drug molecules were charged). However, other effects would require altering the model to such an extent as to accommodate for stochastic processes such as degradation of the hydrogel, or thermal variations in the location of obstacles, etc. Nevertheless, we have demonstrated the usefulness of this powerful technique in being able to tailor a hydrogel platform to obtain a specific drug delivery profile.

This thesis provided advancement in our knowledge related to characterizing drug release profiles as well as brought forth a novel technique to be used in controlling drug delivery profiles. The results presented in this thesis with respect to the characterization of drug release profiles can serve as a practical guide to experimentalists faced with the task of comparing various hydrogels and their associated release profiles. We have presented practical suggestions in order to reliably use the Weibull and the Peppas functions. We have also shown the effectiveness of our combinatorial approach to designing drug delivery platforms. It is hoped that this thesis may serve as the foundation for future studies and refinements to our current drug delivery model.

6

References

[1] *Fortune 500 2006: Top Performers*, ***http://money.cnn.com/magazines/fortune/fortune500/performers/industries/return_on_revenues/index.html*** (accessed 2 August 2006).

[2] C Brunk. *Food, health, and biotechnology: Consumer and social issues in Canada's new food and health product industries.* In *Overview of New Food and Health Products Industries in Canada.* Centre for Studies in Religion and Society, (24 August 2006).

[3] M Snir, S Otto, S Huss-Lederman, D Walker, J Dongarra. *MPI: the complete reference.* The MIT Press, Cambridge (1998).

[4] RS Langer, NA Peppas. *Present and future applications of biomaterials in controlled drug delivery systems,* ***Biomater.*** **2**, 201–214 (1981).

[5] RS Langer, J Folkman. *Polymers for the sustained release of proteins and other macromolecules,* ***Nature*** **263**, 797–800 (1976).

[6] RS Langer, DA Tirrell. *Designing materials for biology and medicine,* ***Nature*** **428**, 487–492 (2004).

[7] NA Peppas, P Bures, W Leobandung, H Ichikawa. *Hydrogels in pharmaceutical formulations,* ***Eur. J. Pharm. Biopharm.*** **1**, 27–46 (2000).

[8] B Jeong, YH Bae, DS Lee, SW Kim. *Biodegradable block copolymers as injectable drug-delivery systems,* ***Nature*** **388**, 860–862 (1997).

[9] NA Peppas, JJ Sahlin. *Hydrogels as mucoadhesive and bioadhesive materials: a review,* ***Biomater.*** **17**, 1553–1561 (1996).

[10] NA Peppas, AR Khare. *Preparation, structure and diffusional behavior of hydrogels in controlled release,* ***Adv. Drug Del. Rev.*** **11**, 1–35 (1993).

[11] K Kataoka, A Harada, Y Nagasaki. *Block copolymer micelles for drug delivery: design, characterization and biological significance*, ***Adv. Drug. Del. Rev.*** **47**, 113–131 (2001).

[12] WM Saltzman, WL Olbricht. *Building drug delivery into tissue engineering*, ***Nature Rev. Drug Disc.*** **1**, 177–186 (2002).

[13] LC Dong, AS Hoffman. *A novel-approach for preparation of ph-sensitive hydrogels for enteric drug delivery*, ***J. Contr. Rel.*** **15**, 141–152 (1991).

[14] "Polymers in Controlled drug delivery". *Medical Device Link*, ***http://www.devicelink.com/mpb/archive/97/11/003.html*** (accessed 2 August 2006).

[15] HL Frisch. *Sorption and transport in glassy polymers – a review*, ***Polym. Engin. Sci.*** **20**, 2–13 (1990).

[16] "Fick's law of diffusion". *Wikipedia*, ***http://en.wikipedia.org/wiki/Fick%27s_law*** (accessed 21 July 2006).

[17] "Brownian motion". *Wolfram research*, ***http://scienceworld.wolfram.com/physics/BrownianMotion.html*** (accessed 21 July 2006).

[18] S Redner. *A guide to first-passage processes*. Cambridge University Press, New York (2001).

[19] A Einstein. *On the movement of small particles suspended in stationary liquids required by the molecular-kinetic theory of heat*, ***Ann. Phys.*** **17**, 549–560 (1905).

[20] PG De Gennes. *La percolation: un concept unificateur*, ***La Recherche.*** **7**, 919–927 (1976).

[21] S Havlin, D Ben-Avraham. *Diffusion in disordered media*, ***Adv. Phys.*** **36**, 695–798 (1987).

[22] S Havlin, A Bunde. *Fractals and Disordered Systems*. Springer-Verlag, Berlin (1996).

[23] PJ Reynolds, HE Stanley, W Klein. *Large-cell Monte Carlo renormalization group for percolation*, ***Phys. Rev. B*** **21**, 1223 (1980).

[24] MJ Saxton. *Anomalous diffusion due to obstacles: a Monte Carlo study*, ***Biophys. J.*** **66**, 394–401 (1994).

[25] D Stauffer, A Aharony. *Introduction to Percolation Theory*. Taylor & Francis, London (1992).

[26] H Juárez, G Rico, L Villafuerte. *Influence of admixed carboxymethylcellulose on release of 4-aminonpyridine from hydroxypropyl methylcellulose matrix tablets*, ***Int. J. Pharm.*** **216**, 115–125 (2001).

[27] Ghez R. *A Primer of Diffusion Problems*. John Wiley & Sons, Inc., New York (1988).

[28] EW Montroll, GH Weiss. *Random walks on lattices II*, ***J. Math. Phys*** **6**, 167–181 (1965).

[29] CW Gardiner. *Handbook of Stochastic Methods*. Springer-Verlag, Berlin (1990).

[30] I Majid, DB Avraham, S Havlin, HE Stanley. *Exact-enumeration approach to random walks on percolation clusters in two dimensions*, ***Phys. Rev. B*** **30**, 1626–1628 (1984).

[31] RB Pandey, D Stauffer. *Confirmation of dynamical scaling at the percolation threshold*, ***Phys. Rev. Lett.*** **51**, 527–529 (1983).

[32] MJ Saxton. *Anomalous subdiffusion in fluorescence photobleaching recovery: A monte carlo study*, ***Biophys. J.*** **81**, 2226–2240 (2001).

[33] K Binder, DW Heermann. *Monte Carlo simulation in statistical physics*. Springer-Verlag, New York (1992).

[34] "Markov property". *Wikipedia*, ***http://en.wikipedia.org/wiki/Markovian*** (accessed 27 July 2006).

[35] DC Hong, S Havlin, HJ Herrmann, HE Stanley. *Breakdown of Alexander-Orbach conjecture for percolation conductivity*, ***Phys. Rev. B*** **30**, 4083–6 (1984).

[36] P Meakin, HE Stanley. *Spectral Dimension for the Diffusion-Limited Aggregation Model of Colloid Growth*, ***Phys. Rev. Lett.*** **51**, 1457–1460 (1983).

[37] S Havlin, GH Weiss, JE Kiefer, M Dishon. *Exact enumeration of random walks with traps*, ***J. Phys. A*** **17**, L347–L350 (1984).

[38] S Havlin, M Dishon, JE Kiefer, GH Weiss. *Trapping of Random Walks in Two and Three Dimensions*, ***Phys. Rev. Lett.*** **53**, 407–410 (1984).

[39] JF Mercier, GW Slater. *Numerically exact diffusion coefficients for lattice systems with periodic boundary conditions. i. theory*, ***J. Chem. Phys.*** **110**, 6050 (1999).

[40] JF Mercier, GW Slater. *Numerically exact diffusion coefficients for lattice systems with periodic boundary conditions. ii. numerical approach and applications*, ***J. Chem. Phys.*** **110**, 6057 (1999).

[41] ThM Nieuwenhuizen, PFJ van Velthoven, MH Ernst. *Diffusion and long-time tails in a two-dimensional site-percolation model*, ***Phys. Rev. Lett.*** **57**, 2477–2480 (1986).

[42] J Crank. *The Mathematics of Diffusion*. Clarendon Press, Oxford (1975).

[43] "Genetic algorithm". *Wikipedia*, ***http://en.wikipedia.org/wiki/Genetic_algorithm*** (accessed 24 July 2006).

[44] JH Holland. *Outline for a Logical Theory of Adaptive Systems*, ***J. Assoc. Comput. Mach.*** **9**, 297–314 (1962).

[45] DB Fogel. *An evolutionary approach to the traveling salesman problem*, ***Biol. Cybern.*** **60**, 139–144 (1988).

[46] LYO Li, Z Fu. *The school bus routing problem: a case study*, ***J. Oper. Res. Soc.*** **53**, 552–558 (2002).

[47] T Back, M Schutz. *Intelligent mutation rate control in canonical genetic algorithms*. In *Int. Symp. on Method. for Intelligent Sys.*, pages 158–167, (1996).

[48] P Chelminiak, RE Marsh, JA Tuszyński. *Asymptotic time dependence in the fractal pharmacokinetics of a two-compartment model*, ***Phys. Rev. E*** **72**, 031903 (2005).

[49] DL Elbert, AB Pratt, MP Lutolf, S Halstenberg, JA Hubbell. *Protein delivery from materials formed by self-selective conjugate addition reactions*, ***J. Contr. Rel.*** **76**, 11–25 (2001).

[50] RM Barrer. *A new approach to gas flow in capillary systems*, ***J. Phys. Chem.*** **57**, 35–40 (1953).

[51] T Higuchi. *Rate of release of medicaments from ointment bases containing drugs in suspension*, ***J. Pharm. Sci.*** **50**, 874 (1961).

[52] RK Korsmeyer, R Gurny, E Doelker, P Buri, NA Peppas. *Mechanisms of solute release from porous hydrophilic polymers*, ***Int. J. Pharm.*** **15**, 25–35 (1983).

[53] V Papadopoulou, K Kosmidis, M Vlachou, P Macheras. *On the use of the Weibull function for the discernment of drug release mechanisms.*, ***Int. J. Pharm.*** **309**, 44–50 (2005).

[54] W Weibull. *A statistical distribution function of wide applicability*, ***J. Appl. Mech.*** **18**, 293–297 (1951).

[55] "Waloddi Weibull". *Wikipedia*, ***http://en.wikipedia.org/wiki/Waloddi_Weibull*** (accessed 4 August 2006).

[56] F Langenbucher. *Linearization of dissolution rate curves by the weibull distribution*, ***J. Pharm. Pharmacol.*** **24**, 979 (1972).

[57] K Kosmidis, P Argyrakis, P Macheras. *A reappraisal of drug release laws using Monte Carlo simulations: The prevalence of the Weibull function*, ***Pharm. Res.*** **20**, 988–995 (2003).

[58] T Schreiner, UF Schaffer, H Loth. *Immediate drug release from solid oral dosage forms*, ***J. Pharm. Sci.*** **94**, 120–133 (2004).

[59] P Costa, JMS Lobo. *Modeling and comparison of dissolution profiles*, ***Pharm. Sci.*** **13**, 123–133 (2001).

[60] A Bunde, S Havlin, R Nossal, HE Stanley, GH Weiss. *On controlled diffusion-limited drug releas from a leaky matrix*, ***J. Chem. Phys.*** **83**, 5909–5914 (1985).

[61] A Dokoumetzidis, K Kosmidis, P Argyrakis, P Macheras. *Modeling and Monte Carlo simulations in oral drug absorption*, ***Basic Clin. Pharm. Tox.*** **96**, 200–205 (2004).

[62] P Lánský, M Weiss. *Classification of dissolution profiles in terms of fractional dissolution rate and a novel measure of heterogeneity*, ***J. Pharm. Sci.*** **92**, 1632–1647 (2003).

[63] N Metropolis, S Ulam. *The Monte Carlo method*, ***J. Am. Stat. Assoc.*** **44**, 335–341 (1949).

[64] M Matsumoto, T Nishimura. *Mersenne twister: a 623-dimensionally equidistributed uniform pseudo-random number generator*, ***ACM Trans. Model. Comp. Sim.*** **8**, 3–30 (1998).

[65] N Metropolis, AW Rosenbluth, MN Rosenbluth, AH Teller, E Teller. *Equation of state calculations by fast computing machines*, ***J. Chem. Phys.*** **21**, 1087–1092 (1953).

[66] S Shenker, J Tobochnik. *Monte Carlo renormalization-group analysis of the classical Heisenberg model in two dimensions*, ***Phys. Rev. B*** **22**, 4462–4472 (1980).